Intracellular Acetyl CoA Potentiates the Therapeutic Efficacy of Antitumor CD8$^+$ T Cells

Snehanshu Chowdhury[1,2], Anwesha Kar[1,2], Debaleena Bhowmik[2,3], Anupam Gautam[4,5], Debashree Basak[1,2], Ishita Sarkar[1,2], Puspendu Ghosh[1], Deborpita Sarkar[1], Alvina Deka[6], Paramita Chakraborty[7], Asima Mukhopadhyay[8], Shikhar Mehrotra[7], Soumen Basak[6], Sandip Paul[9], and Shilpak Chatterjee[1,2]

ABSTRACT

Effector CD8$^+$ T cells rely primarily on glucose metabolism to meet their biosynthetic and functional needs. However, nutritional limitations in the tumor microenvironment can cause T-cell hyporesponsiveness. Therefore, T cells must acquire metabolic traits enabling sustained effector function at the tumor site to elicit a robust antitumor immune response. Here, we report that IL12-stimulated CD8$^+$ T cells have elevated intracellular acetyl CoA levels and can maintain IFNγ levels in nutrient-deprived, tumor-conditioned media (TCM). Pharmacological and metabolic analyses demonstrated an active glucose–citrate–acetyl CoA circuit in IL12-stimulated CD8$^+$ T cells supporting an intracellular pool of acetyl CoA in an ATP-citrate lyase (ACLY)–dependent manner. Intracellular acetyl CoA levels enhanced histone acetylation, lipid synthesis, and IFNγ production, improving the metabolic and functional fitness of CD8$^+$ T cells in tumors. Pharmacological inhibition or genetic knockdown of ACLY severely impaired IFNγ production and viability of CD8$^+$ T cells in nutrient-restricted conditions. Furthermore, CD8$^+$ T cells cultured in high pyruvate–containing media *in vitro* acquired critical metabolic features of IL12-stimulated CD8$^+$ T cells and displayed improved antitumor potential upon adoptive transfer in murine lymphoma and melanoma models. Overall, this study delineates the metabolic configuration of CD8$^+$ T cells required for stable effector function in tumors and presents an affordable approach to promote the efficacy of CD8$^+$ T cells for adoptive T-cell therapy.

Significance: IL12-mediated metabolic reprogramming increases intracellular acetyl CoA to promote the effector function of CD8$^+$ T cells in nutrient-depleted tumor microenvironments, revealing strategies to potentiate the antitumor efficacy of T cells.

Introduction

Immune checkpoint blockade and adoptive T-cell therapy have yielded remarkable clinical successes (1, 2). However, the efficacy is restricted hitherto to a small fraction of patients with malignancies (3). The major impediment to effective T-cell–based immunotherapy of cancer is the dysfunctionality of T cells in the tumor microenvironment (TME). Myriad immunosuppressive signals, including expression of coinhibitory receptors, scant of essential nutrients, suppressive soluble mediators, etc., have been shown to encumber the effector functions of T cells, particularly IFNγ production in the TME (4–6). Therefore, devising strategies enabling CD8$^+$ T cells to overcome the immunosuppressive barriers in TME is pivotal for favorable T-cell response in cancer.

It is well recognized that the functionality of T cells is inextricably linked with cellular metabolism (7). The distinctive role of aerobic glycolysis has well been demonstrated in promoting IFNγ production by T cells that facilitate their effector function against invading pathogens and tumors (8, 9). In TME, T cells encounter severe metabolic stress due to the high metabolic demand of growing tumor cells, which consequently impinge on the tumoricidal response of T cells (5). It appears that improving the metabolic fitness of CD8$^+$ T cells to maintain IFNγ production in nutrient-depleted TME is pivotal in eliciting a durable antitumor response (10–12). However, understanding the cellular features that ensure effective metabolic adaptability and retention of IFNγ production by CD8$^+$ T cells in TME remains elusive.

Multiple studies have shown that IL12 can augment the therapeutic efficacy of antitumor T cells (13). Although systemic administration of IL12 resulted in dose-related toxicities in clinical trials (14), different strategies focusing on local delivery of IL12 at the tumor site have generated potent antitumor T-cell response (15). In fact, the success of anti-PD1 therapy for cancer has also been shown to be improved by the active maintenance of a positive feed-forward loop of IL12 and IFNγ, secreted by tumor-infiltrating dendritic cells and T cells, respectively (16). Together, these studies indicate a crucial role of IL12 in instilling T cells with cellular features essential for their effector function at the tumor site.

[1]Division of Cancer Biology and Inflammatory Disorder, IICB-Translational Research Unit of Excellence, CSIR-Indian Institute of Chemical Biology, Kolkata, India. [2]Academy of Scientific and Innovative Research (AcSIR), Ghaziabad, India. [3]Division of Structural Biology and Bioinformatics, CSIR-Indian Institute of Chemical Biology, Kolkata, India. [4]Institute for Bioinformatics and Medical Informatics, University of Tübingen, Tübingen, Germany. [5]International Max Planck Research School "From Molecules to Organisms," Max Planck Institute for Biology Tübingen, Tübingen, Germany. [6]System Immunology Laboratory, National Institute of Immunology, New Delhi, India. [7]Department of Surgery, Medical University of South Carolina, South Carolina, Charleston. [8]Department of Gynecological Oncology, Chittaranjan National Cancer Institute, Kolkata, India. [9]Center for Health Science and Technology, JIS Institute of Advanced Studies and Research, JIS University, Kolkata, India.

Note: Supplementary data for this article are available at Cancer Research Online (http://cancerres.aacrjournals.org/).

A. Kar and D. Bhowmik contributed as co-second authors of this article.

Corresponding Author: Shilpak Chatterjee, CSIR-Indian Institute of Chemical Biology, 4 Raja S.C Mallick Road, Kolkata 700032, India. Phone: 33-2499-5700, ext. 3013; E-mail: schatterjee@iicb.res.in

Cancer Res 2022;82:2640–55

doi: 10.1158/0008-5472.CAN-21-4052

Herein, we examined whether the metabolic configuration of IL12-stimulated $CD8^+$ T cells orchestrates a robust antitumor response. Our data indicate that $CD8^+$ T cells stimulated with IL12 can sustain their IFNγ production even in tumor-conditioned media (TCM), which presumably is the key to their robust antitumor response. We find that an IL12-driven increase in the intracellular acetyl CoA level is crucial for retaining the effector function of $CD8^+$ T cells in TCM. Moreover, by promoting lipid synthesis, intracellular acetyl CoA levels maintain the bioenergetics of $CD8^+$ T cells in TCM. Therefore, we propose that strategies to elevate the intracellular acetyl CoA pool in $CD8^+$ T cells will have therapeutic potential to promote T-cell function in cancer.

Materials and Methods

Mice

C57BL/6 mice were housed in the CSIR-Indian Institute of Chemical biology (CSIR-IICB) animal facility. OT-1 and Pmel-1 mice were obtained from The Jackson Laboratory. Animals were maintained in pathogen-free facilities and experimental procedures were approved by CSIR-IICB Institutional Animal Ethics Committee. For tumor experiments, equal number of age and gender-matched (both male and female) mice were randomly assigned for the experiments when they were between 8 and 10 weeks old. No influence of sex on the result of the studies was observed.

Cell lines

EL4-OVA (E.G7-OVA), B16-F10, and HEK293T were obtained from the ATCC. EL4 was obtained from National Center for Cell Science. All the cell lines tested negative for *Mycoplasma* using MycoAlert Mycoplasma Detection Kit (Lonza). Cells between 4 and 6 passages were used in the study.

Collection of ascitic fluid from patients bearing ovarian cancer

Peritoneal ascitic fluid was collected from patients bearing ovarian cancer by medical personnel on obtaining informed consent from patients, with ethical approval from the Institutional Review Board of CSIR-Indian Institute of Chemical Biology, Kolkata, India (Ref. No. IICB/IRB/2020/2P) and Chittaranjan National Cancer Institute, Kolkata India (Ref No. CNCI-IEC-AM-2020–11).

Preparation of TCM

EL-4 (1×10^6) tumor cells were injected subcutaneously into the flank of wild type C57BL/6 mice. Tumors were harvested as they reached 300–400 mm^2 in size and the single-cell suspension was prepared. Cells were plated at 1×10^7 cells/mL in complete RPMI-1640 media and kept overnight in CO_2 incubator. The next day, culture media were collected, centrifuged, and filtered before being stored in aliquots at −80°C for future use.

T-cell culture condition

Naive $CD8^+$ T cells were purified from total splenocytes of 6–9 weeks C57BL/6 mice using Dynabeads Untouched Mouse $CD8^+$ T-cell isolation kit (Invitrogen). Purified naive $CD8^+$ T cells or total splenocytes from C57BL/6 mice were activated with plate-bound anti-CD3 (5 μg/mL) and anti-CD28 (2 μg/mL) either in the presence of IL2 (100 U/mL) or IL12 (10 ng/mL) for three days in complete RPMI supplemented with 10% FBS (Invitrogen). In the case of IL2 Py cells, T cells were activated in glucose-free media containing 5 mmol/L pyruvate supplemented with 10% FBS. After 3 days of activation, $CD8^+$ T cells were either kept in the complete media or 80% TCM overnight. In some cases, purified human $CD8^+$ T cells were activated for 3 days and kept overnight in ascitic fluid obtained from ovarian tumor-bearing patients. In some experiments, *in vitro* differentiated $CD8^+$ T cells were either treated with the vehicle control or 2-deoxy glucose (2DG; 1 mmol/L added on day 0) or iodoacetate (IAA; 5 μmol/L added on day 0) or oxalate (OXA; 20 μmol/L added on day 0) or BMS-303141 (20 μmol/L added on day 0) or UK5099 (20 μmol/L added on day 0) or orlistat (100 μmol/L added on day 3) or rotenone (1 μmol/L added on day 1) or antimycin A (1 μmol/L added on day 1) or oligomycin (1 μmol/L added on day 1).

Adoptive T-cell therapy protocol

EL-4.OVA tumor cells (1×10^6) or B16-F10 melanoma (0.5×10^6 cells) were injected subcutaneously into the left flank of 7–10 weeks old C57BL/6 mice. After 9 days of tumor establishment, *ex vivo* activated OT-1 T cells or gp100 reactive Pmel-1 T cells at 0.5×10^6 cells/mouse were adoptively transferred intravenously into tumor-bearing recipients.

Lentiviral transduction of T cell

One day before transfection, 15×10^6 HEK293T Cells (ATCC) were seeded in 25 mL complete DMEM on 150×25 mm style dishes (Falcon). HEK293T cells were transfected with lentiviral plasmid DNA encoding *m-Acly* shRNA (Origene) or scrambled negative shRNA (Origene) along with structural plasmid ps-PAX2 and p-MD2G using $CaCl_2$ and HBS method. After 24 hours, the medium was replaced with low serum-containing media. 4 hours after media change, sodium butyrate was added at 5 mmol/L conc. and the cells were incubated for additional 72 hours, after which, lentivirus-containing supernatant was collected and filtered. The viral content was concentrated using LentiX Concentrator (Takara Bio) as per the manufacturer's protocol and stored in aliquots at −80°C until used. Freshly isolated mouse $CD8^+$ T cells were activated with anti-mCD3/CD28 coated plate for 48 hours in the presence of IL12 (10 ng/mL) at 37°C incubator. 48 hours after activation, cells were collected, washed, and transferred onto nontissue culture–treated 24-well plates (Falcon) coated overnight with Retronectin (Takara Bio). Cells were transduced with concentrated lentiviral supernatants and spinoculated at 1,000 × *g* for 2 hours at 32°C. IL12 was added to the wells in the said amount after spinoculation and incubated at 37°C for another 48 hours. After the said time period, cells were collected and used for downstream analysis.

Flow cytometry

Staining for cell surface markers was performed by incubating cells with the antibody at 1:200 dilutions in FACS buffer (0.5% BSA, 0.1% Sodium azide in PBS) for 30 minutes at 4°C. For intracellular cytokine staining of IFNγ, surface markers were stained before fixation/permeabilization (BD Cytofix/Cytoperm Kit, BD Biosciences). For staining of transcription factors (T-bet) and histone acetylation (Ac-H3K9, Ac-H3K27), cells were stained with surface markers and fixed/permeabilized with a FoxP3 staining buffer set (eBioscience). Fixable samples were fixed using 1% paraformaldehyde in FACS buffer. Intracellular neutral lipid content was measured by incubating the cells with BODIPY (500 nm; Invitrogen) for 30 minutes at 37°C followed by surface staining with fluorochrome-conjugated antibodies. Samples were acquired on BD LSRFortessa and analyzed with

Table 1. Antibodies used for staining and T-cell activation *in vitro*.

Antibodies	Source	Clone# and Cat#
Anti-mouse CD3	BioXcell	Clone: 145–2C11; Cat# BE001–1
Anti-mouse CD28	BioXcell	Clone: 37.51; Cat# BE0015–1
Anti-human CD3	BioXcell	Clone: OKT-3; Cat# BE001–2
Anti-human CD28	BioXcell	Clone: 9.3; Cat# BE0248
CD4-PE/Cy7	Thermo Fisher Scientific	Clone: GK1.5; Cat# 25–0041–82
CD8-AF700	Thermo Fisher Scientific	Clone: 53–6.7; Cat# 56–0081–82
T-bet-Percp/Cy5.5	Thermo Fisher Scientific	Clone: 4B10; Cat# 45–5825–82
IFNγ-eF660	Thermo Fisher Scientific	Clone: XMG1.2; Cat# 50–7311–82
IFNγ-APC	Thermo Fisher Scientific	Clone: XMG1.2; Cat# 17–7311–82
CD25-APC	Thermo Fisher Scientific	Clone: PC61.5; Cat# 17–0251–82
CD44-Percp/Cy5.5	Thermo Fisher Scientific	Clone: IM7; Cat# 45–0441–82
CD62L-eF450	Thermo Fisher Scientific	Clone: MEL-14; Cat# 48–0621–82
VB5.1/5.2 TCR-FITC	Thermo Fisher Scientific	Clone: MR9–4; Cat# 11–5796–82
CD8-APC/Cy7	Thermo Fisher Scientific	Clone: 53–6.7; Cat# A15386
CD4-BUV 395	BD Biosciences	Clone: GK1.5; Cat# 563790
CD8-Percp/Cy5.5	BD Biosciences	Clone: 53–6.7; Cat# 551162
CD62L-PE	BD Biosciences	Clone: MEL-14; Cat# 553151
Anti-human CD4-Percp/Cy5.5	BD Biosciences	Clone: RPA-T4; Cat# 560650
Anti-human CD8-AF700	BD Biosciences	Clone: OKT-8; Cat# 557945
Anti-human CD4-BUV395	BD Biosciences	Clone: RPA-T4; Cat#564724
Anti-human IFNγ-APC	Invitrigen	Clone: 4S.B3; Cat# 17–7319–82
Anti-human CD8-AF488	Biolegend	Clone: HIT8a; Cat#300916
CD8-FITC	Biolegend	Clone: 53–6.7; Cat# 100706
Acetyl-Histone H3 (Lys9)-Alexa Fluor 647	Cell Signaling Technology	Clone: C5B11; Cat# 4481
Acetyl-Histone H3 (Lys27)-Alexa Fluor 488	Cell Signaling Technology	Clone: D5E4; Cat# 15485

FlowJo software (BD Biosciences). See **Table 1** for antibodies used for staining and T-cell activation *in vitro*.

qRT-PCR

For quantitative RT-PCR (qPCR) cells were lysed using TRIzol reagent (Invitrogen), and RNA was isolated as per TRIzol extraction protocol. RNA was resuspended in UltraPure water (Invitrogen) and quantified on a Biotek Synergy HT Plate Reader. cDNA was generated from 1μg of isolated RNA using the iScript cDNA Synthesis kit (Bio-Rad), and diluted 1:3 in nuclease-free water for qPCR reactions. qPCR was done using iTaq Universal SYBR Green Supermix (Bio-Rad) at standard reaction speed on a CFX96 Real Time System (Bio-Rad) for 40 cycles. All primer sequences are listed in **Table 2**.

Glucose uptake and metabolic flux assay

Glucose uptake was evaluated by labeling the cells with fluorescent-labeled deoxy-glucose analogue, 2NBDG (Cayman Chemicals) according to the manufacturer's protocol followed by surface staining with fluorochrome-conjugated antibodies. Cells were then acquired by flow cytometry (LSRFertessa, BD Biosciences) and data were analyzed with FlowJo software (BD Biosciences).

Table 2. Primer sequences.

Mouse qPCR primers: 5′-3′			
Gene	**Forward**	**Reverse**	**Source**
Glut1	CAGTTCGGCTATAACACTGGTG	GCCCCCGACAGAGAAGATG	IDT, Coralville
HKI	CGGAATGGGGAGCCTTTGG	GCCTTCCTTATCCGTTTCAATGG	IDT, Coralville
HKII	GGAACCGCCTAGAAATCTCC	GGAGCTCAACCAAAACCAAG	IDT, Coralville
Pfk	AGGAGGGCAAAGGAGTGTTT	TTGGCAGAAATCTTGGTTCC	IDT, Coralville
Enol	AAAGATCTCTCTGGCGTGGA	CTTAACGCTCTCCTCGGTGT	IDT, Coralville
Ldha	TGTCTCCAGCAAAGACTACTGT	GACTGTACTTGACAATGTTGGGA	IDT, Coralville
Fasn	GGAGGTGGTGATAGCCGGTAT	TGGGTAATCCATAGAGCCCAG	Eurofins, Luxembourg
Acaca	ATGGGCGGAATGGTCTCTTTC	TGGGGACCTTGTCTTCATCAT	Eurofins, Luxembourg
Srebp1	GATGTGCGAACTGGACACAG	CATAGGGGGCGTCAAACAG	Eurofins, Luxembourg
Acly	CAGCCAAGGCAATTTCAGAGC	CTCGACGTTTGATTAACTGGTCT	Eurofins, Luxembourg
β–Actin	ACGTAGCCATCCAGGCTGGTG	TGGCGTGAGGGAGAGCAT	Eurofins, Luxembourg

Human qPCR primers: 5′-3′			
Gene	**Forward**	**Reverse**	**Source**
Acly	ATCGGTTCAAGTATGCTCGGG	GACCAAGTTTTCCACGACGTT	Eurofins, Luxembourg

Extracellular acidification rate (ECAR) and oxygen consumption rate (OCR) were determined using the Seahorse XFe24 analyzer (Agilent Technologies). Briefly, $CD8^+$ T cells (0.5×10^6 cells/well) were plated on Cell-Tak (CORNING) coated Seahorse culture plate for 30 minutes. ECAR was measured under basal conditions and in response to glucose (10 mmol/L), oligomycin (1.0 μmol/L), and 2-DG (100 mmol/L; Sigma-Aldrich). OCR analysis was carried out under basal conditions and in response to oligomycin (Oligo, 1 μmol/L), fluoro-carbonyl cyanide phenylhydrazone (FCCP, 1 μmol/L) and rotenone plus antimycin A (Rot+ Anti A, 2 μmol/L+ 100 nmol/L). In some cases, OCR analysis was performed in glucose-free media under basal conditions or in response to different concentrations of etomoxir (Eto) followed by oligomycin (1 μmol/L), FCCP (1 μmol/L), and rotenone plus antimycin A (2 μmol/L+ 100 nmol/L).

Cytotoxicity assay

EL4-OVA (specific target) cells labeled with CTV (Invitrogen) were either kept untreated or cocultured with OVA-specific OT-1 T cells activated in different conditions as indicated in **Fig. 1**. After 6 hours of coculture, cells were collected, washed twice in PBS, and acquired by flow cytometry (LSRFortessa, BD Biosciences). CTV labeled EL4 cells (nonspecific target) were also cocultured similarly as described above. Antigen-specific T-cell–mediated tumor cell killing was determined by the decrease in the number of CTV-gated cells.

Acetyl CoA assay

Fluorometric-based determination of intracellular acetyl CoA level was performed in activated $CD8^+$ T cells (1×10^6 cells/group) using the Acetyl-CoA Assay Kit (Sigma-Aldrich) following the manufacturer's protocol. Briefly, activated $CD8^+$ T cells from the indicated groups were collected, washed twice in PBS, and lysed in 1% NP40 in ice for 20 minutes with mixing every 5 minutes. Following lysis, supernatants were collected by centrifugation at 14,000 rpm for 10 minutes at 4°C. Acetyl CoA level was measured in the supernatant following the manufacturer's protocol and readouts were taken using the Varioskan LUX Multimode reader (Thermo Fisher Scientific).

ATP assay

Bioluminescence-based determination of intracellular ATP level was carried out in activated $CD8^+$ T-cell (1×10^6 cells/group) using ATP Bioluminescent Assay Kit (Sigma-Aldrich) according to the manufacturer's protocol. Cell lysis and supernatant collection were done following the same method as described previously in the acetyl CoA assay. ATP level was measured instantly in the supernatant following the manufacturer's protocol and readouts were taken using the Varioskan LUX Multimode reader (Thermo Fisher Scientific).

Glucose, glutamine, and lactate assay

Complete RPMI and TCM were diluted in PBS (250-fold dilution for glucose, 50-fold dilution for glutamine and 100-fold dilution for lactate assay) and glucose, glutamine and lactate levels were measured by Glucose-Glo Assay kit (Promega), Glutamine/Glutamate-Glo Assay kit (Promega), and Lactate- Glo Assay kit (Promega), respectively. For differential glucose uptake study following activation, T cells were washed twice in glucose-free media following incubation in the same media for 30 minutes and then incubated for 45 minutes in RPMI-1640 media containing 10 mmol/L glucose. After 45 minutes of culture, cells were pelleted down and media were used to assess unconsumed glucose left out in the media. All assays were performed according to the manufacturer's protocol. Luminescence was measured in the Varioskan LUX Multimode reader (Thermo Fischer Scientific).

Dialysis of TCM

TCM was dialyzed with 3.5kDa Slide-A-Lyzer Dialysis Cassette Kit (Thermo Fisher Scientific) according to the manufacturer's protocol. Briefly, the dialysis cassettes were hydrated with water for 2 minutes before use. Cassettes were injected with TCM and dialyzed against complete RPMI overnight at 4°C. TCM inside the membrane was collected, filtered, and used in experiments.

Immunoblotting

For evaluation of Tbet expression, cells were lysed using RIPA buffer containing protease inhibitor cocktail (Thermo Fisher Scientifiic) and total protein was isolated. Equal amounts of proteins (20 μg) were separated by 10% SDS-PAGE and then transferred to nitrocellulose membranes. The membranes were probed with anti-Tbet antibody (Invitrogen) overnight at 4°C followed by incubation with secondary antibody (horseradish peroxidase (HRP)–conjugated goat anti-mouse IgG at 1:10,000 dilutions; Jackson Immuno Research Laboratories) for 2 hours at room temperature. Prestained protein markers (Invitrogen) were run in parallel to identify the molecular weight of proteins. For chemiluminescent detection, the membranes were treated with Clarity Western ECL substrate (Bio-Rad), and the signal was monitored using Bio-Rad Versadoc Imaging System (Bio-Rad). The same membrane was stripped with stripping buffer and reprobed with antibody specific to β-actin (Cell Signaling Technology) as a reference control.

Chromatin immunoprecipitation assay

To perform the assay, approximately 1×10^7 IL12-stimulated mouse $CD8^+$ T cells were used. The processing was done with SimpleChIP Enzymatic Chromatin IP Kit (9003s; Cell Signaling Technology) according to the manufacturer's protocol. Briefly, cells were fixed with 1% paraformaldehyde (w/v) and crosslinked with glycine. Nuclei preparation and chromatin digestion were performed using two separate buffers with DTT. Chromatin IPs were done in 1X chromatin immunoprecipitation (ChIP) buffer with Ac-H3K9 antibody (9649s; Cell Signaling Technology) or normal rabbit immunoglobulin G (IgG) as control for overnight at 4°C following mixing with ChIP-Grade Protein G Magnetic beads for 2 hours at 4°C. Chromatin was eluted after heating the sample at 65°C for 30 minutes. Reverse cross-link was performed with 5 mol/L NaCl and Proteinase K. DNA was purified in different buffers using spin columns and eluted in the elution buffer supplied with the kit. Agarose gel PCR was performed to test the quality of desired DNA products. qPCR was performed in SYBR Green–based method with the IP DNA, IgG and 2% input samples. PCR primers for the ChIP assay spanned nonrepetitive conserved genomic sequences (mouse and human) from about 70 kb upstream to about 60 kb downstream of the *Ifng* gene (17). Dissociation curves after amplification showed that primer pairs generated single products. Percentage of input was calculated with the method provided in the kit protocol.

ELISA

The assay was performed with IFNγ Mouse Uncoated ELISA Kit (Invitrogen) as per the manufacturer's protocol. Briefly, the ELISA plates were coated overnight with capturing antibody. After blocking the plates, samples and standards were added and incubated for 2 hours at room temperature. Cytokine amounts were detected by anti-IFNγ detection antibody followed by the addition of HRP-conjugated streptavidin and 1x Tetramethylbenzidine substrate

solution. The quantification was done as per the protocol using the standard curve.

Metabolomics and stable isotope tracing analysis

Intracellular metabolites were determined by performing metabolomics analysis using UPHPLC/MS/MS and GC/MS platform (Metabolon Inc.). Data were then grouped by unsupervised clustering using MetaboAnalyst software. Samples were loaded equivalently across the platform and normalized to Bradford values before statistical analysis.

For, stable isotope tracer analysis, both IL2 and IL12-stimulated $CD8^+$ T cells (5×10^6 cells/group) were cultured for 6 hours in glucose-free RPMI (with 10% dialyzed FBS) containing 10 mmol/L $^{13}C_6$ glucose (Cambridge Isotope Laboratories). Metabolites were extracted using ice clod 80% methanol, followed by three freeze-thaw cycles in dry ice. Cellular debris were removed by centrifugation at 14,000 rpm for 10 minutes at 4°C and supernatant was collected and stored in −80°C unit used. An untargeted metabolomics service to trace ^{13}C incorporation in TCA cycle metabolites was provided by Novelgene Technologies, India. Briefly, a sample of 10 μL was injected into a Shimadzu Prominence-I HPLC (Shimadzu Corporation) interfaced to a Shimadzu triple quadrupole LCMS-8045 mass spectrometer (Shimadzu Corporation). The electrospray ionization (ESI)–MS analysis was performed in both positive and negative ion modes. Full-scan mass spectra were acquired over a mass range of m/z 50–1900. For untargeted LC-MS generated files, initially, each file (.mzXML format) was separated into two based on their ionization mode by using XMCS (18). DeltaMS (19) isotope signature module was then used on each set of files (positive and negative) to carry out isotope tracing. In it for light isotope C12 and heavy C13 were chosen, and for peak, detection polarity was adjusted depending on the ionization mode of files, remaining settings were kept on default. Reported mz values (for both positive and negative ionization mode files) were queried for the compound by using the HMDB (20) database with molecular weight tolerance ± 0.05, and the mode was adjusted, respectively.

HDAC activity assay

For HDAC activity assay, 3 days activated purified mouse $CD8^+$ T cells were taken in 1.5×10^6 cells per replicate. Nuclear proteins were isolated using the nuclear extraction buffer and an equal amount of protein was used to determine HDAC activity using Epigenase HDAC Activity/Inhibition Direct Assay Kit (Colorimetric; EPIGENTEK) following to the manufacturer's protocol.

RNA sequencing and analysis

Each sample, containing 1.5×10^6 cells was dissolved in 1 mL TRIzol (Invitrogen) and shipped in dry ice to MedGenome Laboratories for mRNA sequencing. Briefly, RNA was isolated from TRIzol samples using QIAGEN RNeasy Mini Kit (Qiagen, Cat# 74104) The extracted RNA samples were quantified using Qubit HS RNA Assay (Invitrogen, Cat# Q32855). RNA purity was checked using QIAxpert and the integrity was assessed on TapeStation using RNA HS Screen Tapes (Agilent, Cat# 5067–5579). NEB Ultra II Directional RNA-Seq Library Prep kit protocol was used to prepare libraries for total RNA sequencing (NEB, Cat# E7760L). cDNAs were made from purified mRNAs using reverse transcriptase followed by PCR. PCR products are then purified using Agencourt AMPure beads (Beckman Coulter, Cat# A63882) and checked for fragment size distribution on Fragment Analyzer using HS NGS Fragment Kit (1–6000bp; Agilent, Cat# DNF-474–1000). Prepared libraries were quantified using Qubit HS Assay (Invitrogen, Cat# Q32854). The obtained libraries were pooled and diluted to the final optimal loading concentration before cluster amplification on the Illumina flow cell. Once the cluster generation was completed, the cluster flow cell was loaded on the Illumina HiSeq X instrument to generate 50 mol/L, 150bp paired end reads.

Twelve samples belonging to four treatment groups (three samples for each group) were selected for RNA-seq analysis. The treatment groups are IL2, IL2 80% (IL2+80% TCM), IL12, and IL12 80% (IL12+80% TCM). The quality of the raw, paired-ended fastq files were checked using FastQC (Available online at: http://www.bioinformatics.babraham.ac.uk/projects/fastqc/) and then mapped against *Mus musculus* GRCm38 genome using STAR aligner (v2.27.2b; ref. 21). The resulting bam files were further processed using Rsamtools, Rsubread (22) and GenomicAlignments R packages (23) to obtain an abundance table. This abundance table was first normalized and then used to identify the differentially abundant genes with the help of the DESeq2 R package (24). Only those genes with an adjusted $P < 0.05$ were considered for further downstream analysis. For the construction of the heatmaps, first, the genes were checked that overlapped between the different treatment groups, and then the genes of interest were selected; following that the raw values of the abundance table were normalized using counts per million normalization of edgeR package (25) and then visualized with pheatmap package.

The gene set enrichment analysis was done on the differential genes obtained from DESeq2 analysis, based upon the 4 groups, using the fgsea R package against the hallmark gene set of the MSigDB database.

Statistical analysis

All data reported are the arithmetic mean from 3 or 5 independent experiments performed in triplicate ± SD unless stated otherwise. Comparisons between two groups were performed using an unpaired, two-tailed, Student *t* test. Comparisons between more than two groups were performed using one-way or two-way ANOVA. Data analyses were performed using the GraphPad Prism 9 software (GraphPad).

Data availability

RNA sequencing data have been deposited in the Gene Expression Omnibus (GEO). GEO accession number GSE189170.

Results

IL12 imparts stable effector function in $CD8^+$ T cells in nutrient-deprived condition

Because IL12-primed intratumoral T cells exhibited improved therapeutic response, we wanted to evaluate whether IL12 stimulation could help in retaining the effector function of $CD8^+$ T cells in nutrient-exhausted TME. To model TME *in vitro*, we used TCM, generated by overnight culturing single-cell suspension of EL-4 solid tumor resected from tumor-bearing B6 mice. We observed that overnight TCM exposure drastically curtailed the IFNγ protein and *Ifng* mRNA expression in $CD8^+$ T cells stimulated with IL2; however, no overt decrease was evident for IL12-stimulated $CD8^+$ T cells (**Fig. 1A** and **B**; Supplementary Fig. S1A), even when the cells were exposed for 48 hours in TCM (Supplementary Fig. S1B). Moreover, increasing the concentration of IL2 either during stimulation or during exposure to TCM could not restore the ability of $CD8^+$ T cells to maintain IFNγ production in TCM. In contrast, IL12, even at a lower concentration, exhibited effector function in TCM (Supplementary Fig. S1C and S1D). Akin to polyclonally stimulated $CD8^+$ T cells, MHC class I restricted OVA-specific OT-1 T cells activated with its cognate antigen ($OVA_{257–264}$) in the presence of IL12 also exhibited sustained IFNγ production in 80% TCM, whereas a striking drop in IFNγ production was noted for IL2-stimulated $CD8^+$ T cells

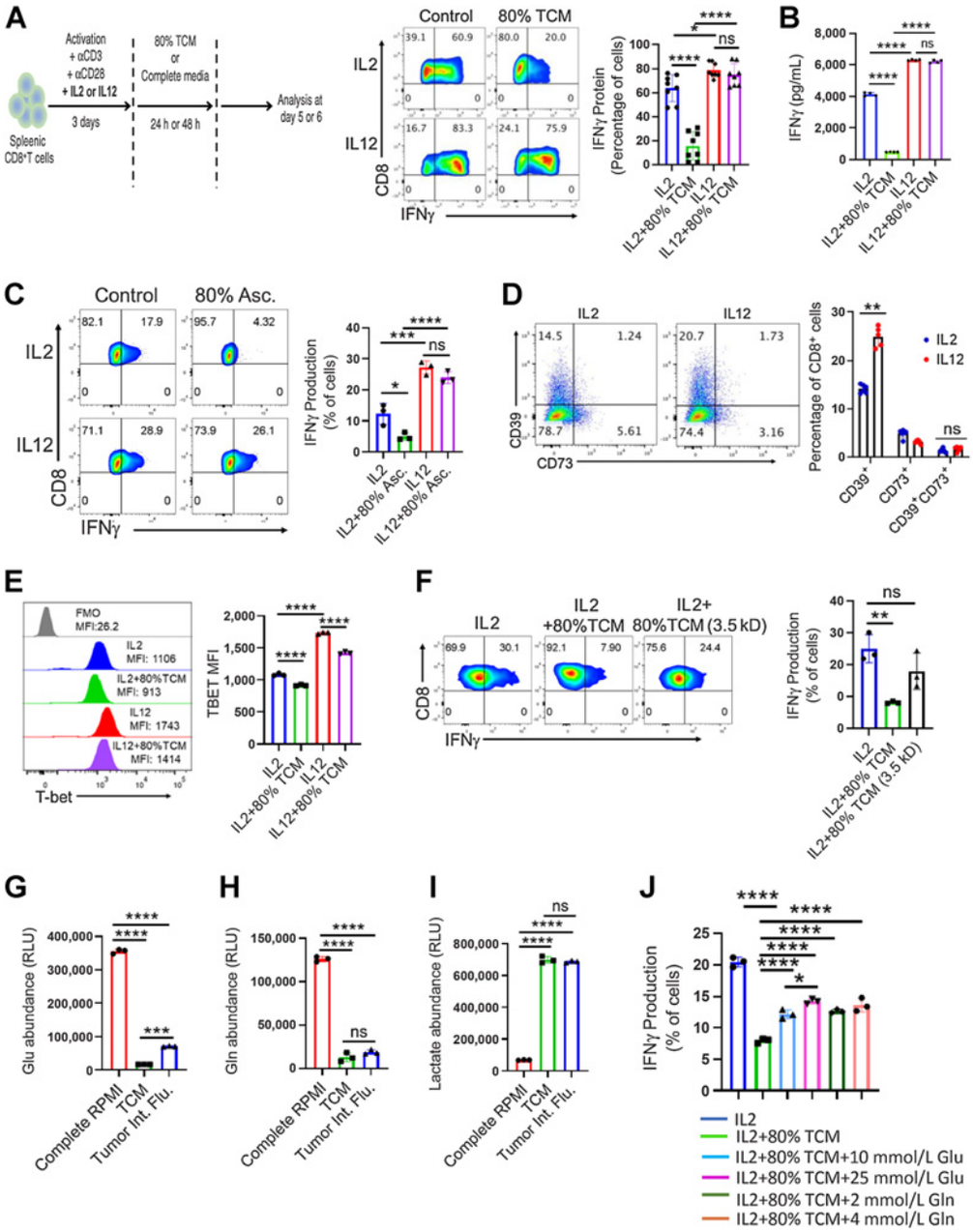

Figure 1.

Sustained IFNγ production by IL12-stimulated CD8$^+$ T cells in TCM. **A** and **B,** CD8$^+$ T cells were activated for 3 days, followed by overnight exposure in either 80% TCM or complete media before being assessed for IFNγ production by flow cytometry (**A**) and ELISA (**B**). Adjacent scatter plot of **A** represents the frequency of IFNγ-producing CD8$^+$ T cells. **C,** Human CD8$^+$ T cells were activated for 3 days before being exposed overnight in 80% ascitic fluid (obtained from ovarian tumor-bearing patients)–containing media. Adjacent scatter plot represents the frequency of IFNγ-producing CD8$^+$ T cells. **D,** Flow cytometry–based evaluation of the frequency of CD8$^+$ T cells expressing CD39 and CD73. Adjacent bar diagram represents the cumulative data from three independent experiments. **E,** Intracellular expression of T-bet in IL2- and IL12-stimulated CD8$^+$ T cells with or without overnight exposure in 80% TCM. Adjacent bar diagram represents the cumulative data of mean fluorescence intensity (MFI). **F,** Intracellular IFNγ production by IL2-stimulated CD8$^+$ T cells cultured overnight either in complete RPMI, or 3.5kDa dialyzed TCM or undialized TCM. Adjacent bar diagram represents the frequency of IFNγ-producing CD8$^+$ T cells. **G–I,** Biochemical measurement of glucose (Glu; **G**), glutamine (Gln; **H**), and lactate (**I**) levels in TCM, EL-4 tumor interstitial fluid, and complete RPMI. **J,** Assessment of intracellular IFNγ production by IL2-stimulated CD8$^+$ T cells either in complete RPMI, or 80% TCM, or 80% TCM supplemented with the indicated concentration of glucose and glutamine. Data are representative of eight (**A**), four (**B**), three (**C, E, F, G, H, I,** and **J**), and five independent experiments (**D**). *, $P < 0.05$; **, $P < 0.01$; ***, $P < 0.005$; ****, $P < 0.0001$; ns, nonsignificant.

(Supplementary Fig. S1E). A similar observation was also noted for human $CD8^+$ T cells stimulated with IL12 followed by exposure to media containing 80% ovarian tumor ascitic fluid (**Fig. 1C**). Furthermore, we found that brief exposure to TCM significantly subverted the cytotolytic potential of IL2-stimulated OT-1 cells *in vitro* against EL4-OVA, whereas no such decrease was evident for IL12-stimulated OT1 T cells (Supplementary Fig. S1F).

Next, we attempted to identify whether there were any phenotypic differences between IL2 and IL12-stimulated $CD8^+$ T cells, which potentially contribute to differential effector response in TCM. Evaluating the frequencies of cells coexpressing CD39 and CD73, ectoenzymes that promote the generation of immunosuppressive adenosine (26), demonstrated no notable difference between IL2 and IL12-stimulated $CD8^+$ T cells (**Fig. 1D**). Furthermore, both the activation states as discerned by the frequencies of effector memory ($CD44^+$) and central memory ($CD44^+CD62L^+$) populations (Supplementary Fig. S1G), and proliferation potential were comparable between IL2 and IL12-stimulated $CD8^+$ T cells (Supplementary Fig. S1H). Finally, we tested the involvement of T-bet, a key transcription factor driving IFNγ production by T cells. Although T-bet expression was approximately 1.5-fold higher in IL12-stimulated $CD8^+$ T cells as compared with IL2-stimulated cells, both the cell types exhibited a significant drop in T-bet expression after overnight exposure to TCM (**Fig. 1E**; Supplementary Fig. S1I). A similar finding was also noted for Eomes (Supplementary Fig. S1J), a paralogue of T-bet, which has been found to invoke IFNγ production in $CD8^+$ T cells (27). Our data suggested that sustained IFNγ production by IL12-stimulated $CD8^+$ T cells in TCM was independent of T-bet and EOMES expression.

Next, we explored whether the observed loss of IFNγ production by IL2-stimulated $CD8^+$ T cells, but not by IL12-stimulated cells, was in part due to depletion of nutrients in TCM. To investigate this, we first dialyzed TCM against a large volume of complete RPMI using a 3.5 kDa dialysis cassette to equilibrate cellular metabolites between these media (RPMI→ TCM), while retaining protein fraction in the TCM (28). Interestingly, we found that IFNγ production was partially restored in IL2-stimulated $CD8^+$ T cells exposed overnight in dialyzed TCM (**Fig. 1F**), indicating that nutrient limitation in TCM primarily accounted for this effect as no difference in protein concentration between un-dialyzed and dialyzed TCM was observed (Supplementary Fig. S1K). Furthermore, we noted that glucose and glutamine, two important metabolites crucial for T cells effector function, were severely depleted in TCM and the levels were comparable with tumor interstitial fluid (**Fig. 1G** and **H**). On the contrary, immunosuppressive metabolite lactate was several folds higher in both TCM and tumor interstitial fluid than complete RPMI (**Fig. 1I**). Finally, repleting either glucose or glutamine in TCM could partially restore IFNγ production by IL2-stimulated cells (**Fig. 1J**). These data together suggest that nutrient stress, especially depletion of glucose and glutamine in TME, hinders the effector function of IL2-stimulated $CD8^+$ T cells. However, activation of $CD8^+$ T cells in the presence of IL12 instills the cells with the ability to sustain their effector function in nutrient-restricted TCM.

IL12 upregulates the expression of genes associated with glucose and lipid metabolism in $CD8^+$ T cells

To elucidate the mechanism of how IL12 stimulation endows $CD8^+$ T cells to retain their IFNγ production in TCM, we carried out RNA-seq analysis of both IL2 and IL12-stimulated cells with or without exposure in 80% TCM (mentioned as TCM hereafter). Principal-component analysis revealed a discrete transcriptomic profile in each group (**Fig. 2A**). Furthermore, we performed the comparative transcriptomics analyses among four different conditions viz: IL12 TCM versus IL2 TCM, IL12 versus IL2, IL12 TCM versus IL12, and IL2 TCM versus IL2 to identify commonly deregulated genes in TCM condition as well as in IL12. For each comparison, the differentially expressed genes (DEG; Supplementary Fig. S2A; Supplementary Table S1 for up and down DEGs) and subsequently the upregulated (**Fig. 2B**) and downregulated (Supplementary Fig. S2B) DEGs for four different comparisons were identified. The pathway enrichment analysis for these comparisons yielded common upregulation of the Cholesterol Homeostasis hallmark pathway in IL2 TCM and IL12 TCM groups compared with IL2 and IL12 groups, respectively (Supplementary Fig. S3A). At the same time, the Hallmark Estrogen Response Late (Genes defining late response to estrogen) pathway was commonly enriched in IL12 and IL12 TCM groups compared with IL2 and IL2 TCM groups, respectively (Supplementary Fig. S3A). We mainly focused on DEGs that were commonly upregulated in IL12 and IL12 TCM groups in the present study. We argued that these commonly upregulated genes would reflect important biochemical pathway(s) and signaling molecules crucial for maintaining the effector function of $CD8^+$ T cells in a nutrient-depleted TME. Of note, a cohort of 292 common DEGs were upregulated in IL12 and IL12 TCM groups as compared with IL2 and IL2 TCM groups, respectively (**Fig. 2B**), indicating an IL12-specific transcriptional signature that remained unaffected in TCM and could be decisive in instilling the effector features into $CD8^+$ T cells. We also noted a cohort of 183 DEGs, which were upregulated in the IL12 group when compared with the IL2 group, but mainly were enriched in the IL12 TCM group relative to the IL2 TCM group or IL12 group, indicating that the transcriptional signature of TCM exposed IL12-stimulated $CD8^+$ T cells (**Fig. 2B**).

Upon analysis of 292 DEGs, we found that a few genes associated with glycolysis (*Hk2, Slc2a1, chst2,* and *prps1*) were highly upregulated in IL12-stimulated $CD8^+$ T cells, even when cells were exposed to 80% TCM (**Fig. 2C**). In addition, genes associated with the IFNγ response and TNFα signaling were highly enriched in both IL12 and IL12 TCM groups (**Fig. 2C**). Notably, genes involved in promoting antitumor immunity and long-lasting memory formation (*CD28, ID2, P2rx7,* and *Stat5a*) were also found to be upregulated in both IL12 and IL12 TCM groups (**Fig. 2C**; refs. 11, 29–31). We also noticed high *Hlx* expression in IL12-stimulated $CD8^+$ T cells, which could aid in augmenting IFNγ production by T cells in 80% TCM (32).

Analysis of 183 DEGs revealed that a few genes related to lipid metabolism and fatty acid synthesis pathway (*Acaca, Scd1, Scd2, Fads2, Elovl6,* and *Pltp*), were primarily upregulated in IL12 TCM $CD8^+$ T cells (**Fig. 2D**). The data indicate a crucial role of lipid metabolism in supporting the bioenergetic needs of IL12-stimulated $CD8^+$ T cells in the TCM (33, 34). Furthermore, we noted that genes upregulated in the IL12 TCM condition were also involved in positive costimulation (*Icos*), NAD^+ biosynthesis (*Naprt*), mTOR signaling (*Hif1a*), and dephosphorylation of Akt (*Phlpp1*; **Fig. 2D**), all of which have been reported to promote antitumor responses of T cells (35–37). Importantly, we found that the expression of *Tpp2* involved in the stabilization of HK2 by interfering with lysosomal degradation (38), was also upregulated in IL12 TCM $CD8^+$ T cells (**Fig. 2D**), highlighting a critical mechanism underlying steady glycolysis in IL12-stimulated $CD8^+$ T cells even when they were exposed to the nutrient-restricted condition. Together, our data indicate a distinct transcriptional signature of IL2 and IL12 $CD8^+$ T cells, which could in part be responsible for differential effector response in the nutrient-restricted tumor milieu.

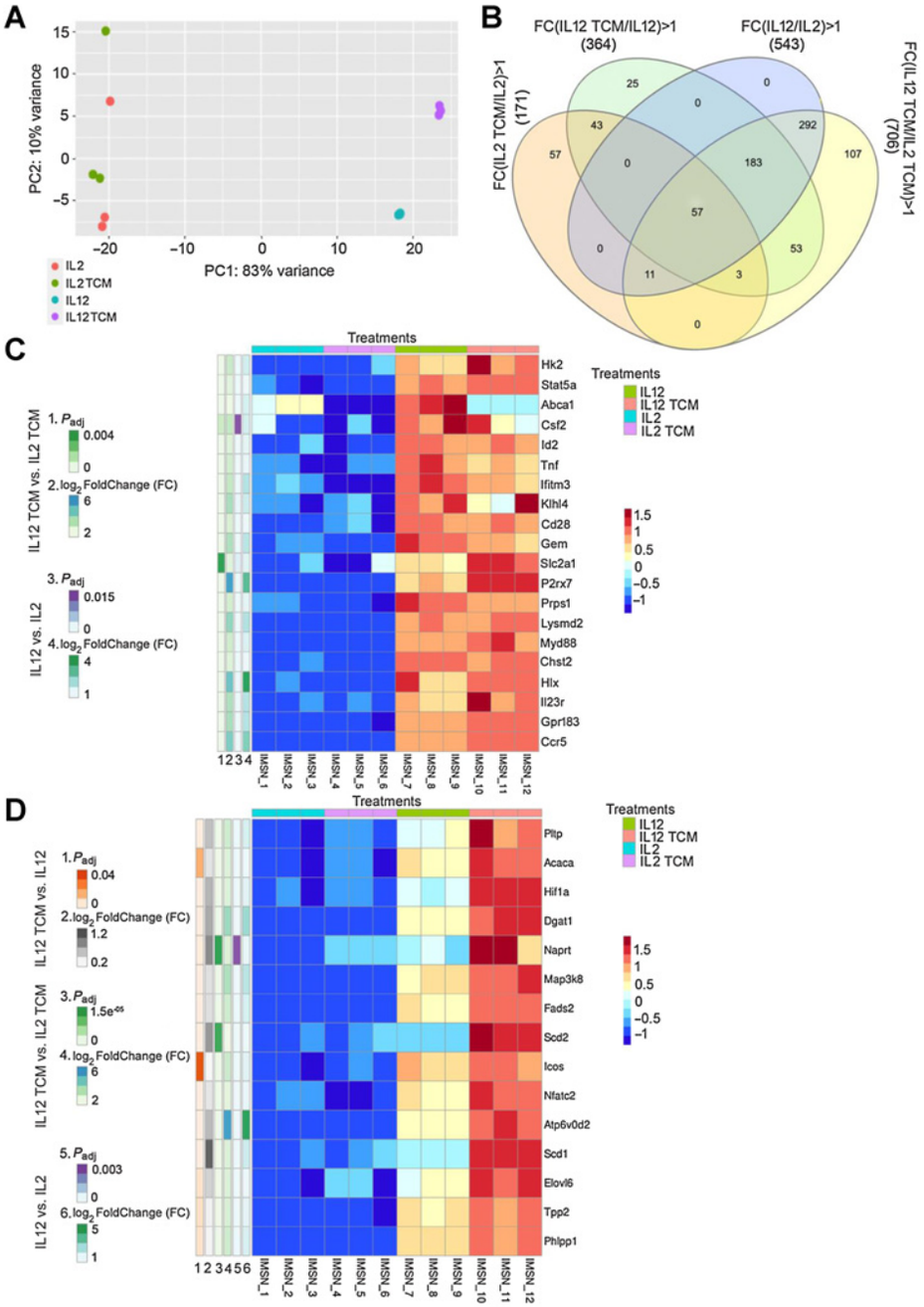

Figure 2.

Distinct transcriptional profile of IL2- and IL12-stimulated CD8$^+$ T cells exposed overnight in either complete media or 80% TCM. **A,** PCA plot depicting the distribution of the gene profile of each sample from four different groups. **B,** Venn diagram showing the overlap of upregulated DEGs between each group (P_{adj} <0.05). **C,** Heatmap showing the expression of selected genes from 292 upregulated DEGs common between IL2 versus IL12 and IL2 TCM versus IL12 TCM. **D,** Heatmap showing the expression of selected genes from 183 upregulated DEGs common between IL2 versus IL12, IL2 versus IL12 TCM, and IL12 versus IL12 TCM. Fold change represents fold change on a $\log_2$ scale, whereas P_{adj} represents the adjusted *P* value.

Glucose metabolism through glycolysis is essential for IL12-stimulated CD8$^+$ T cells to retain their IFNγ production in TCM

Given the enrichment of glycolysis-associated genes in IL12-stimulated CD8$^+$ T cells, we next sought to determine the relevance of glucose metabolism in conferring stable effector function in IL12-stimulated cells in TCM. Upon assessing glycolytic potential, we observed that both glucose uptake (**Fig. 3A** and Supplementary S4A) and ECAR, a direct measure of glycolysis, were significantly higher in IL12-stimulated CD8$^+$ T cells as compared with IL2-stimulated cells (**Fig. 3B**). Most intriguingly, TCM exposure sharply decreased the overall glycolysis (**Fig. 3C**) and glycolytic capacity of IL2-stimulated cells, whereas a moderate decrease was observed in the case of IL12-stimulated CD8$^+$ T cells (**Fig. 3D**). Moreover, genes encoding molecules of the glycolytic pathway were highly upregulated in both IL12 and TCM-exposed IL12-stimulated CD8$^+$ T cells but severely affected in IL2-stimulated CD8$^+$ T cells exposed to TCM (**Fig. 3E**; Supplementary Table S2). In addition to glycolysis, mitochondrial respiration was found to be significantly impaired in IL2-stimulated CD8$^+$ T cells exposed overnight in 80% TCM, whereas, it was minimally affected in TCM exposed IL12-stimulated CD8$^+$ T cells (**Fig. 3F** and **G**). The data indicate that IL12-stimulated CD8$^+$ T cells are more metabolically resilient than IL2-stimulated cells, and that might help in maintaining their IFNγ response in TCM.

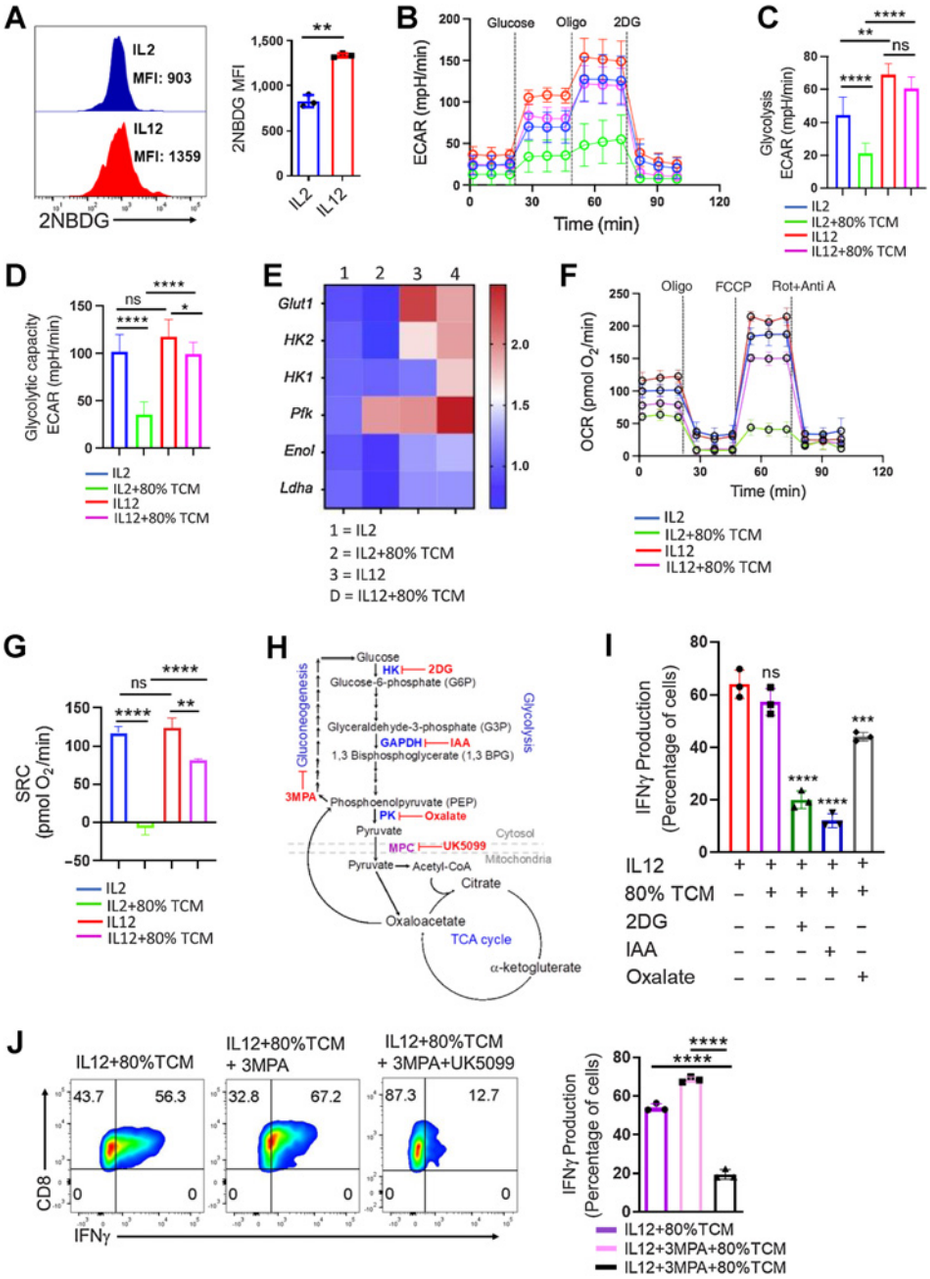

Figure 3.

Increased glucose catabolism through glycolysis sustains IFNγ production by IL12-stimulated CD8$^+$ T cells in TCM. **A,** Glucose uptake by 2-NBDG. Adjacent scatter plot represents the cumulative data of mean fluorescence intensity (MFI) from three independent experiments. **B–E,** Activated CD8$^+$ T cells cultured overnight either in 80% TCM or complete media were evaluated for ECAR time course in response to glucose, oligomycin (Oligo), and 2DG (**B**); ECAR level after glucose addition (**C**); glycolytic capacity of the cells (**D**); qPCR analysis of glycolysis associated genes (**E**); OCR under basal condition and in response to indicated inhibitors (**F**); and spare respiratory capacity (SRC; **G**). **H,** Schematic representation of the glucose metabolism pathway and targets of the indicated inhibitors. **I** and **J,** CD8$^+$ T cells were activated with IL12 in the presence or absence of glycolytic inhibitors (2DG, 1 mmol/L; IAA, 5 μmol/L; oxalate, 20 μmol/L; **I**) or mitochondrial pyruvate transporter inhibitor (UK5099, 20 μmol/L) in combination with gluconeogenesis inhibitor (3MPA, 500 μmol/L; **J**) before being evaluated for intracellular IFNγ production in 80% TCM. The scatter plot represents the cumulative data from three independent experiments. *, $P < 0.05$; **, $P < 0.01$; ***, $P < 0.005$; ****, $P < 0.0001$; ns, nonsignificant.

Given the role of glycolysis in regulating IFNγ production by activated T cells, we next interrogated the possible contribution of this pathway in endowing IL12-stimulated CD8$^+$ T cells with the ability to maintain IFNγ production in nutrient-depleted TCM. To address this issue, pharmacological inhibitors blocking hexokinase (using 2DG), glyceraldehyde-3-phosphate dehydrogenase (using iodoacetate) and pyruvate kinase (using oxalate) were used during the stimulation of CD8$^+$ T-cell in the presence of IL12, and IFNγ production was assessed following exposure in TCM (**Fig. 3H**). We observed that blocking glycolysis at any of the intermediate steps although had minimal effect in reducing IFNγ production by complete media exposed cells (Supplementary Fig. S4B), but markedly diminished the ability of IL12-stimulated CD8$^+$ T cells to produce IFNγ in TCM (**Fig. 3I**). Consistent with an earlier study (10), we also observed that inhibition of glycolysis using 2DG early during activation of CD8$^+$ T cells in the presence of IL2 markedly elevated their IFNγ production following restimulation in nutrient-repleted condition (Supplementary Fig. S4C). Overall, the data suggest that metabolic switching to glycolysis during activation was essential for IL12-stimulated CD8$^+$ T cells to acquire the ability to sustain their functionality in TCM. We next questioned whether the oxidation of glycolysis-derived pyruvate in mitochondria had any role in making IL12-stimulated CD8$^+$ T cells functionally active in TCM. Interestingly, we found that blocking pyruvate entry into mitochondrial using UK5099 in the presence of gluconeogenesis inhibitor, 3MPA in IL12-stimulated CD8$^+$ T cells severely impaired their ability to produce IFNγ in 80% TCM (**Fig. 3J**).

These data together suggest that increased glycolytic flux and subsequent pyruvate entry into mitochondria are decisive in endowing IL12-stimulated CD8$^+$ T cells with metabolic fitness crucial for sustaining IFNγ production in nutrient-restricted conditions. This is worth mentioning here that although we found that glycolysis is vital in empowering IL12-stimulated CD8$^+$ T cells to maintain their functionality in TCM, mitochondrial oxidative phosphorylation remained an important checkpoint in regulating the effector function of T cells (Supplementary Fig. S4D) as reported earlier (39, 40).

ACLY-dependent generation of cytosolic acetyl CoA maintains bioenergetic demands and IFNγ production by CD8$^+$ T cells in TCM

To further assess metabolic changes, we performed metabolomics analyses of IL2 and IL12-stimulated CD8$^+$ T cells. Consistent with our gene expression and metabolic flux data, metabolomics analysis also revealed that glycolysis was predominant in IL12-stimulated CD8$^+$ T cells relative to IL2-stimulated cells (**Fig. 4A**). Further analysis of sugar metabolism pathways displayed enrichment of several pentose phosphate pathway (PPP) metabolites in IL12-stimulated CD8$^+$ T cells (**Fig. 4B**), suggesting that glucose allocation to PPP might be involved in improving the antioxidant potential of the cells (41). Most intriguingly, we noticed that although citrate and isocitrate levels were found low in IL12-stimulated CD8$^+$ T cells, acetyl CoA levels were elevated in these cells (**Fig. 4C** and **D**). Similar enrichment of acetyl CoA pool was also noted in human CD8$^+$ T cells stimulated with IL12 (Supplementary Fig. S5A). This observation indicated that citrate was likely being exported out of mitochondria through citrate-malate shuttle and used to generate cytosolic acetyl CoA pool involving a reaction catalyzed by ATP-dependent citrate lyase (ACLY; Supplementary Fig. S5B). Indeed, we found that the expression of *Acly,* the gene encoding the enzyme catalyzing the generation of acetyl CoA and oxaloacetate from citrate and CoA (42), was significantly higher in both mouse and human IL12-stimulated CD8$^+$ T cells as compared with IL2-stimulated CD8$^+$ T cells (**Fig. 4E**; Supplementary Fig. S5C). Remarkably, inhibition of ACLY, either using pharmacological inhibitor BMS303141 or shRNA-mediated knockdown of *Acly* (Supplementary Fig. S5D), significantly reduced intracellular acetyl CoA level in IL12-stimulated CD8$^+$ T cells (Supplementary Fig. S5E and S5F).

Next, to ascertain the contribution of glucose-derived citrate in enriching acetyl CoA pool in IL12-stimulated CD8$^+$ T cells, we performed metabolic-tracing analysis using uniformly labeled $^{13}C_6$ glucose (Supplementary Fig. S5G). Although the analyses could not quantitatively determine labeled metabolites, the pattern depicted a marked increase in ^{13}C-labeled acetyl CoA in IL12-stimulated CD8$^+$ T cells as compared with IL2-stimulated cells (**Fig. 4F**). Next, to interrogate whether citrate was used to enrich the acetyl CoA pool, we analyzed isotopologue distribution in citrate and downstream metabolites (fumarate, malate, and oxaloacetate) in IL12 and IL2-stimulated CD8$^+$ T cells. Our data revealed that although ^{13}C-labeled citrate (m+4 and m+6) was significantly higher in IL12-stimulated CD8$^+$ T cells as compared with IL2-stimulated cells (**Fig. 4G**), no marked difference in ^{13}C-labeled fumarate, malate, and oxaloacetate was observed (**Fig. 4H–J**). We argued that if citrate was fully used in the TCA cycle rather than in generating acetyl CoA pool, then a consistent difference in ^{13}C-labeled metabolites downstream of citrate (like fumarate, malate, and oxaloacetate) would have also been observed between IL2 and IL12-stimulated cells. Collectively, these data suggested that IL12-stimulated CD8$^+$ T cells used glucose-derived citrate to generate cytosolic acetyl CoA pool. The notion was further supported by the observation that CD8$^+$ T cells stimulated with IL12 in the presence of low-glucose media (1 mmol/L glucose) exhibited a significant decrease in acetyl CoA levels as compared with CD8$^+$ T cells stimulated with IL12 in complete media (Supplementary Fig. S5H).

Intracellular acetyl CoA is the major acetyl group donor for histone acetylation, a process known to be associated with transcriptional regulation (43). Recent studies have demonstrated the crucial role of H3K9Ac in regulating the expression of effector response-associated genes, including IFNγ in T cells (44, 45). Herein, we also noted increased histone H3 acetylation at lysine 9 (H3K9Ac) as well as at lysine 27 (H3K27Ac) in IL12-stimulated CD8$^+$ T cells as compared with IL2-stimulated cells (Supplementary Fig. S5I and S5J). To rule out the possibility of differential HDAC activity influencing histone acetylation in IL2 and IL12-stimulated CD8$^+$ T cells, we measured global HDAC activity and found it comparable between the two groups (Supplementary Fig. S5K). Next, to assess the role of ACLY in this context, we blocked ACLY activity using the pharmacological inhibitor BMS303141 and found reduced histone acetylation at both H3K9 and H3K27 (Supplementary Fig. S5L and S5M). Furthermore, CD8$^+$ T cells stimulated with IL12 in low-glucose media also exhibited reduced acetylation of both H3K9 (Supplementary Fig. S5N) and H3K27 (Supplementary Fig. S5O), supporting the role of the glucose–citrate–acetyl CoA circuit in regulating histone acetylation in IL12-stimulated CD8$^+$ T cells. As it has been reported that H3K9Ac at the *Ifng* locus is associated with an active transcription (44, 45), we performed ChIP of H3K9Ac in IL12-stimulated CD8$^+$ T cells and our data revealed a substantial enrichment of H3K9Ac at the *Ifng* locus (Supplementary Fig. S5P; refs. 45, 46). The data suggest that the metabolic circuit described here provides a critical mechanism underpinning sustained IFNγ response by IL12-stimulated CD8$^+$ T cells in TME.

Because we found that intracellular acetyl CoA levels were elevated in IL12-stimulated CD8$^+$ T cells, even after exposure overnight in TCM (Supplementary Fig. S5Q), we, next, interrogated the impact of intracellular acetyl CoA depletion on the effector function of IL12-stimulated CD8$^+$ T cells in TCM. We found that both BMS303141 treatment and shRNA-mediated knockdown of *Acly* compromised the ability of IL12-stimulated CD8$^+$ T cells to maintain IFNγ production in TCM (**Fig. 4K** and **L**). Furthermore, human CD8$^+$ T cells stimulated with IL12 in the presence of BMS303141 also exhibited a considerable drop in IFNγ production in ascetic fluid (Supplementary Fig. S5R). Most intriguingly, inhibition of ACLY substantially decreased the viability of IL12-stimulated CD8$^+$ T cells only when the cells were exposed to TCM, but not in complete media (**Fig. 4M** and **N**; Supplementary Fig. S5S and S5T). Interestingly, the effect was specific to IL12-stimulated cells, as barely any difference in viability was observed when BMS303141-treated IL2-stimulated CD8$^+$ T cells were exposed in TCM (Supplementary Fig. S5U). Moreover, we also observed that CD8$^+$ T cells stimulated with IL12 in presence of low-glucose media exhibited a dramatic drop in viability when exposed to TCM (Supplementary Fig. S5V). Collectively, the data suggest that intercellular acetyl CoA levels not only augment IFNγ production but are also crucial for maintaining the viability of IL12-stimulated CD8$^+$ T cells in TCM.

Cytosolic acetyl CoA is the rate-limiting metabolite for lipid biosynthesis (47), which can be used through lipolysis to fulfill the bioenergetic demands of T cells in nutrient-restricted conditions (33, 34). So, we checked whether the intracellular acetyl CoA pool drove lipid biosynthesis in IL12-stimulated CD8$^+$ T cells, and thereby maintained their cellular viability in TCM. We observed that mRNA expression of *Srebp1* (**Fig. 4O**), the master regulator of *de novo* lipid synthesis, as well as genes encoding enzymes involved in *de novo*

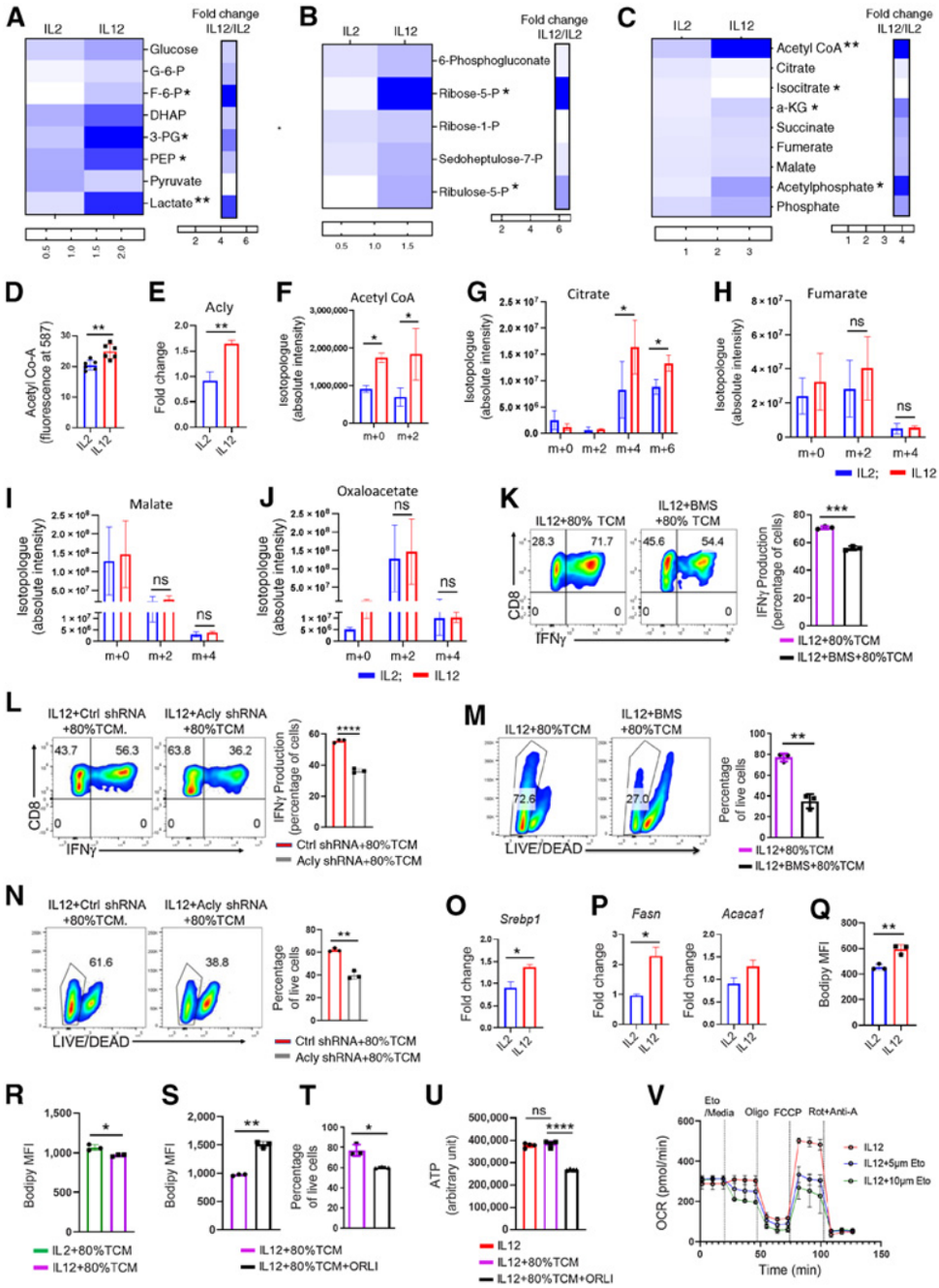

Figure 4.

Intracellular acetyl CoA levels regulate the fate and function of IL12-stimulated CD8$^+$ T cells in TCM. **A–C,** Mass spectrometry–based determination of intracellular metabolite levels of glycolysis (**A**), PPP (**B**), and TCA cycle (**C**). Cumulative data from three biological replicates are shown. **D,** Intracellular acetyl CoA level in IL2- and IL12-stimulated CD8$^+$ T cells. **E,** qPCR analysis of *Acly* expression. **F–J,** Isotopologue distribution for acetyl CoA (**F**), citrate (**G**), fumarate (**H**), malate (**I**), and oxaloacetate (**J**) in CD8$^+$ T cells stimulated either with IL2 or IL12 in a medium containing $^{13}C_6$ glucose. **K–N,** ACLY inhibitor BMS303141-treated or empty vector–transduced or *Acly* shRNA-transduced CD8$^+$ T cells were stimulated with IL12, followed by overnight exposure in 80% TCM and used for evaluation of IFNγ production (**K** and **L**) and percentage of viable cells by flow cytometry–based staining of live/dead dye (**M** and **N**). Adjacent plots represent the cumulative data from three independent experiments. **O** and **P,** CD8$^+$ T cells activated with either IL2 or IL12 were used to evaluate transcript levels of Srebp*1* (**O**), and *Fasn* and *Acaca* (**P**). **Q–S,** Intracellular lipid content using BODIPY was determined in IL2 and IL12-stimulated CD8$^+$ T cells after 3 days of activation (**Q**), both the cell types after overnight exposure in 80% TCM (**R**), and IL12-stimulated CD8$^+$ T cells exposed overnight in 80% TCM ± orlistat (100 μmol/L; **S**). Data are representative of three independent experiments. MFI, mean fluorescence intensity. **T** and **U,** Determination of percentage of viable cells (**T**) and intracellular ATP level (**U**) in IL12-stimulated CD8$^+$ T cells exposed overnight in 80% TCM in the presence or absence of orlistat (100 μmol/L). Data are representative of three independent experiments with similar results. **V,** CD8$^+$ T cells were activated for three days and evaluated for OCR time course in response to different concentrations of etomoxir/media, oligomycin, FCCP and rotenone+antimycin A in glucose-free conditions. *, $P < 0.05$; **, $P < 0.01$; ***, $P < 0.005$; ****, $P < 0.0001$; ns, nonsignificant.

fatty acid synthesis, including *Fasn* and *Acaca,* were highly upregulated in IL12-stimulated CD8$^+$ T cells (**Fig. 4P**). We also found that IL12-stimulated CD8$^+$ T cells had more neutral lipid content than IL2 cells (**Fig. 4Q**). Next, we evaluated the relative potential of these cell types to use their stored lipid when exposed to TCM. We noticed that cellular lipid content was sharply dropped in IL12-stimulated CD8$^+$ T cells when exposed to TCM (**Fig. 4R**); however, the levels could be reverted by blocking lipolysis in this condition (**Fig. 4S**), suggesting that IL12-stimulated cells use lipolysis to use their stored lipid during the nutrient-restricted condition. Most interestingly, we observed that inhibition of lipolysis substantially decreased the viability of IL12-stimulated CD8$^+$ T cells when exposed to 80% TCM but not in complete media (**Fig. 4T**; Supplementary Fig. S5W), suggesting that lipolysis may act as an alternative energy source, which in part meets the bioenergetic requirements of IL12-stimulated CD8$^+$ T cells in nutrient-depleted condition. The notion was further supported by the observation that blocking lipolysis using orlistat significantly reduced the intracellular ATP levels of IL12 CD8$^+$ T cells exposed to 80% TCM (**Fig. 4U**). Moreover, we also found that IL12-stimulated CD8$^+$ T cells maintain high mitochondrial oxidative phosphorylation when measured in glucose-free conditions, but it was severely affected by inhibition of mitochondrial lipid oxidation using etomoxir (**Fig. 4V**). Together these data suggested an intriguing feature of IL12-stimulated CD8$^+$ T cells, positioning acetyl CoA at the intersection of histone modification and lipid biosynthesis, both of which might act in concert to exhibit the durable effector function in TME.

Activation of CD8$^+$ T cells in high pyruvate–containing media mimics the phenotype of IL12-stimulated CD8$^+$ T cells

Next, we reasoned that augmenting pyruvate oxidation in mitochondria would increase cellular acetyl CoA pool through citrate, and hence maintain the effector function of CD8$^+$ T cells in TCM. To address this, purified CD8$^+$ T cells were activated in high pyruvate (5 mmol/L)–containing media (without glucose) to ensure the productive channeling of pyruvate to mitochondria. As observed in the IL12 condition, CD8$^+$ T cells stimulated in 5 mmol/L pyruvate (referred to as IL2 Py cells hereafter), had elevated acetyl CoA levels (**Fig. 5A**) and increased expression of both H3K9Ac (**Fig. 5B**) and H3K27Ac (**Fig. 5C**), as compared with complete media stimulated CD8$^+$ T cells (referred as IL2 cells hereafter). Moreover, depletion of intracellular acetyl CoA level by blocking ACLY using BMS303141 substantially decreased both H3K9 and H3K27 acetylation in IL2 Py CD8$^+$ T cells (**Fig. 5D** and **E**). In addition, we also observed an increased expression of *Acly* in IL2 Py cells as compared with IL2 cells (**Fig. 5F**). Most importantly, akin to IL12-stimulated cells, IL2 Py cells also maintain their IFNγ production when exposed overnight to 80% TCM (**Fig. 5G**), and this effect was intracellular acetyl CoA dependent as its depletion using BMS303141, caused a dramatic drop in IFNγ production in 80% TCM (**Fig. 5H**).

Upon assessing the metabolic features of IL2 Py CD8$^+$ T cells, we noted that the ability to uptake glucose analogue, 2NBDG was significantly higher in IL2 Py cells than in IL2 cells (**Fig. 5I**). Moreover, the expression of genes encoding enzymes of the glycolytic pathway was also upregulated in IL2 Py CD8$^+$ T cells (**Fig. 5J**; Supplementary Table S3). In addition, the expression of genes encoding enzymes involved in *de novo* fatty acid synthesis, including *Srebp1, Fasn* and *Acaca* were also found to be upregulated in IL2 Py cells as compared with IL2 cells (**Fig. 5K**). Consistent with the above observations, IL2 Py cells also exhibited reliance on lipolysis to meet their bioenergetics when the cells were in TCM, as orlistat treatment decreased their ATP level in 80% TCM condition (**Fig. 5L**). These observations pointed to the fact that culturing CD8$^+$ T cells in high pyruvate–containing media in the absence of glucose, instills the cells with vital metabolic features as observed in IL12-stimulated CD8$^+$ T cells.

IL12 and IL2 Py cells exhibit enhanced antitumor response *in vivo*

Given the functional fitness of both IL12 and IL2 Py CD8$^+$ T cells in nutrient-depleted TCM, we, next, sought to determine their antitumor potential upon adoptive transfer into mice bearing EL4-OVA tumors. We found that adoptive transfer of OT1 T cells (0.5×10^6 cells/mouse) stimulated either in IL12 or IL2 Py conditions could efficiently control tumor growth (**Fig. 6A** and **B**), and markedly enhanced the survival of tumor-bearing mice (**Fig. 6C**). Comparing the frequency of tumor epitope-reactive circulating T cells (Vβ5.1$^+$ OT1 T cells) in tumor-bearing host revealed a higher number of Vβ5.1$^+$ T cells in mice who received either IL12 or IL2 Py T cells as compared with mice who received IL2-stimulated cells (**Fig. 6D**). Furthermore, our data suggested that the enhanced tumor control observed with IL12 and IL2 Py–stimulated CD8$^+$ T cells was correlated with their improved persistence and ability to produce IFNγ at the tumor site (**Fig. 6E**). Moreover, we also tested the antitumor efficacy of adoptively transferred IL12 and IL2 Py-stimulated gp100-reactive CD8$^+$ T cells (Pmel-1) in a highly aggressive B16-F10 tumor model. Akin to OT1 T cells, IL12 and IL2 Py-stimulated Pmel-1 T cells displayed durable antitumor response (Supplementary Fig. S6A and S6B) and improved persistence (Supplementary Fig. S6C) in the tumor-bearing host.

Next, we sought to determine the impact of ACLY in regulating the superior antitumor response exhibited by both IL12 and IL2 Py-stimulated CD8$^+$ T cells. Pharmacological inhibition of ACLY using BMS303141 during stimulation of CD8$^+$ T cells either with IL12 or IL2 Py significantly impaired their ability to control subcutaneously established EL4-OVA tumor (**Fig. 6F** and **G**) and survival to tumor-bearing mice (**Fig. 6H** and **I**) upon adoptive transfer. Assessing the persistence and functionality of the adoptively transferred T cells in the tumor-bearing host revealed that ACLY inhibition compromised the ability of IL12 and IL2 Py cells to maintain their IFNγ production and survival at the tumor site (**Fig. 6J** and **K**). Moreover, the frequency of Vβ5.1$^+$ OT1 T cells in the peripheral blood of tumor-bearing mice receiving ACLY inhibitor-treated IL12 or IL2 Py cells were also found to be reduced (Supplementary Fig. S6D and S6E). Together these data suggest that fueling mitochondrial pyruvate oxidation augments the therapeutic potential of antitumor CD8$^+$ T cells in cancer.

Discussion

Metabolic stress is emerging as a critical confounding factor restraining the functionality and persistence of T cells in the tumor (5). Inadequacy of essential nutrients like glucose in TME leaves the tumor-infiltrating T cells metabolically impaired. As a result, T cells infiltrating tumor sites lose their antitumor potential rapidly, leading to incessant tumor growth (5, 48, 49). Therefore, to mount a protective immune response, T cells must adopt a mechanism that could ensure appropriate cellular metabolism underpinning prolonged effector function at the tumor site. Considering the well-appreciated role of IL12 in augmenting the antitumor potential of T cells, we aimed to elucidate the metabolic features essential for carrying out the robust antitumor response of IL12-stimulated CD8$^+$ T cells. Our data place intracellular acetyl CoA as a key metabolite that endues CD8$^+$ T cells with metabolic orientation enabling improved effector function in nutrient-deprived TME.

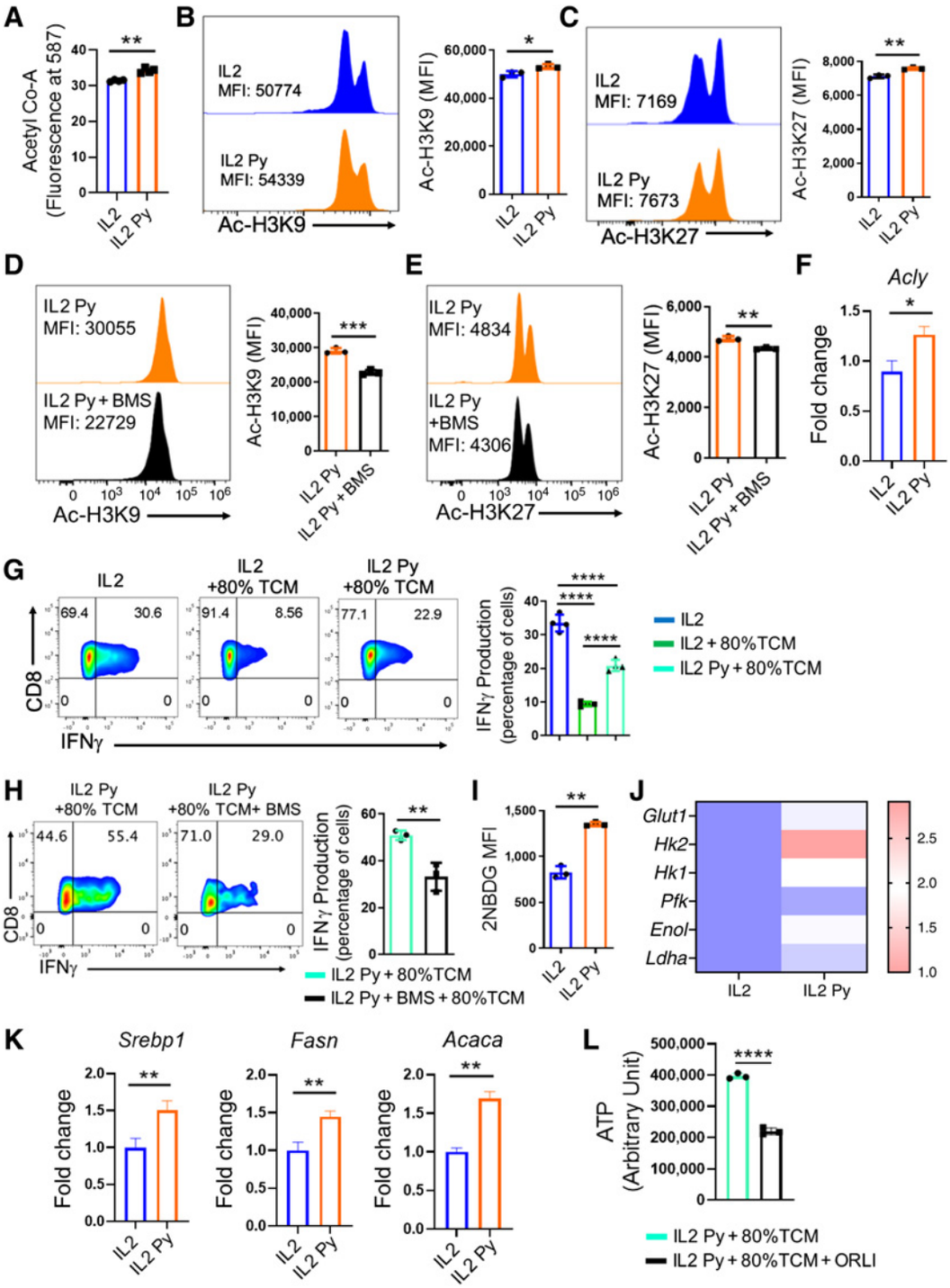

Figure 5.

Activation of CD8$^+$ T cells in high pyruvate–containing media possesses the metabolic traits of IL12-stimulated CD8$^+$ T cells. **A,** CD8$^+$ T cells were activated either in complete media or high pyruvate (5 mmol/L)–containing media (without glucose) and levels of acetyl CoA were measured. Data are representative of three independent experiments with similar results. **B–E, G,** and **H,** CD8$^+$ T cells were activated either in complete media or high pyruvate (5 mmol/L)–containing media (without glucose) ± BMS303141 and evaluated for H3K9Ac level (**B** and **D**), H3K27Ac level (**C** and **E**), intracellular IFNγ production (**G** and **H**) either in complete media or 80% TCM. Adjacent plots represent the cumulative data from three (**B–E** and **H**) and four (**G**) independent experiments. **F** and **I-K,** CD8$^+$ T cells activated either in complete media or high pyruvate–containing media (without glucose) were assessed for transcript level *Acly* (**F**), determination of glucose uptake by 2NBDG (**I**), mRNA expression of various glycolytic genes (**J**), and transcript levels of *Srebp1*, *Fasn,* and *Acaca* (**K**). **L,** Intracellular ATP levels in IL2 Py cells exposed overnight to 80% TCM in the presence or absence of orlistat. Data are representative of three (**F** and **I–L**) independent experiments with similar results. *, $P < 0.05$; **, $P < 0.01$; ***, $P < 0.005$; ****, $P < 0.0001$. MFI, mean fluorescence intensity.

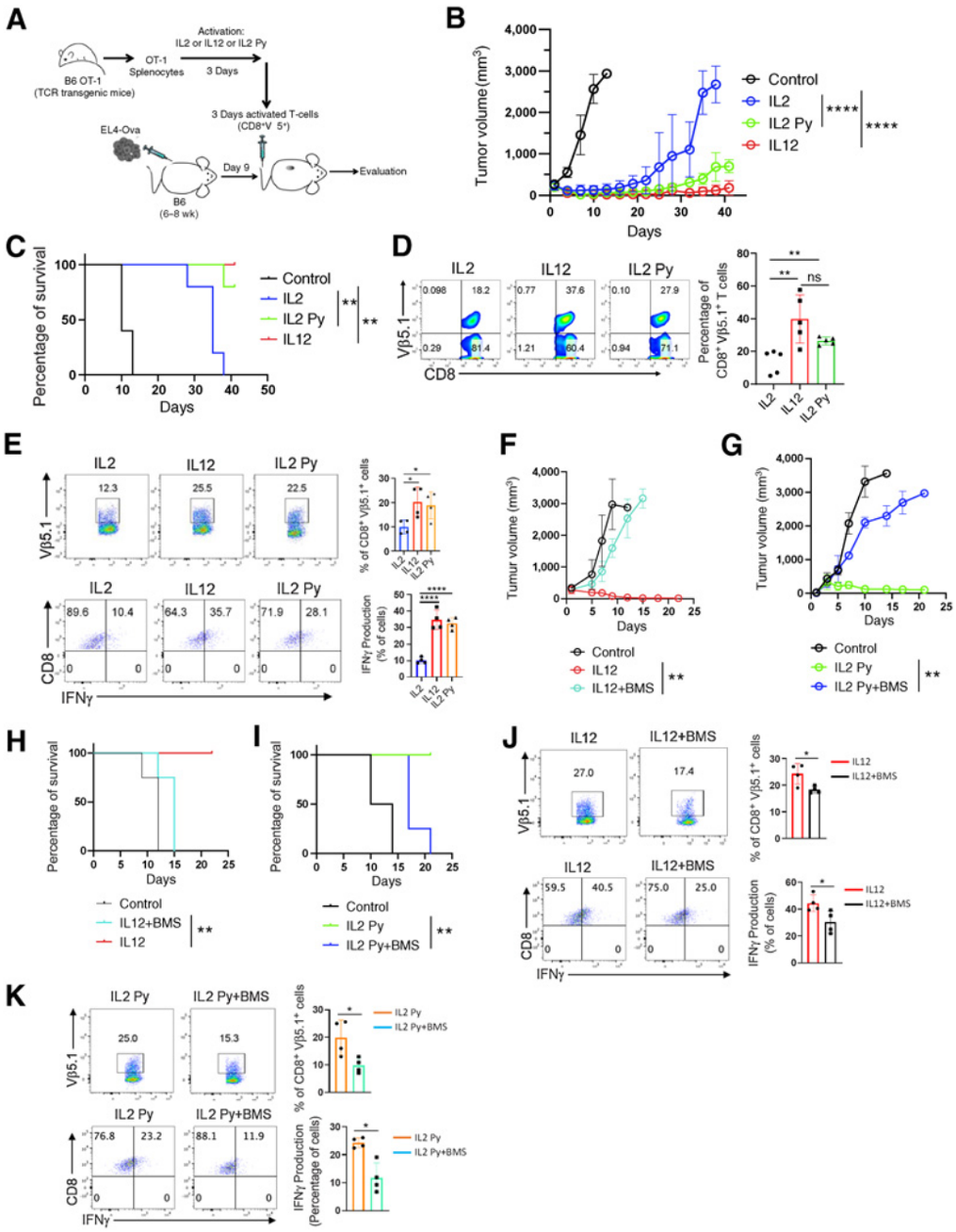

Figure 6.

IL12 and IL2 Py cells exhibit enhanced antitumor response *in vivo*. **A,** Illustration of experimental strategy. **B,** C57BL/6 mice ($n = 5$ mice/group) with 9 days subcutaneously established EL4-OVA tumor were either kept untreated or treated by adoptively transferring (intravenously) 0.5×10^6 OT-1 $CD8^+$ T cells. Tumor growth was measured using a digital caliper every third day. Data in figure demonstrate the mean tumor volume at each time point. **C,** Kaplan–Meier curves for time-to-sacrifice for experimental conditions are shown. **D,** Flow cytometric evaluation of EL4-OVA–specific OT-1 T cells ($v\beta5.1^+CD8^+$ T cells) in the peripheral blood of tumor-bearing mice after 14 days following T-cell transfer. Adjacent bar diagram representing the cumulative data of the percentage of tumor specific OT-1 T cells from tumor-bearing mice ($n = 5$/group). **E,** frequency of adoptively transferred OT1 T cells present at the tumor site (top) and IFNγ production by intratumoral OT1 T cells following restimulation with PMA and ionomycin (bottom). **F–K,** C57BL/6 mice ($n = 4$ mice/group) with subcutaneously established EL4-OVA tumor were adoptively transferred with OT-1 $CD8^+$ T cells stimulated either with IL12 ± BMS303141 or IL2 Py ± BMS303141. **F** and **G,** tumor growth was measured using a digital caliper every third day and the mean tumor volume at each time point is presented. **H** and **I,** Kaplan–Meier curves for time-to-sacrifice for experimental conditions are shown. **J** and **K,** Frequency of adoptively transferred OT1 T cells present at the tumor site (top), and IFNγ production by intratumoral OT1 T cells following restimulation with PMA and ionomycin (bottom) are shown. *, $P < 0.05$; **, $P < 0.01$; ****, $P < 0.0001$; ns, nonsignificant.

One of the key features of IL12-stimulated $CD8^+$ T cells, we noted in our study, was their ability to retain their IFNγ production in nutrient-depleted TCM; the phenomenon appeared to be T-bet independent (32, 50). Metabolic fitness being crucial for T-cell functionality aroused us to speculate that IL12-stimulated $CD8^+$ T cells must have distinctive metabolic traits supporting their IFNγ production in nutrient-limiting conditions. Indeed, we found that elevated intracellular acetyl CoA pool resulting from glucose metabolism to cytosolic citrate was the key pathway for persistent effector function of IL12-stimulated $CD8^+$ T cells in TCM. The notion was supported by the observation that interfering with this metabolic circuit at any step (glycolysis or transportation of pyruvate to mitochondria or depletion of acetyl CoA) resulted in dwindled IFNγ production by IL12-stimulated $CD8^+$ T cells in TCM without affecting their viability (Supplementary Fig. S6F and S6G).

Here, we observed that increased intracellular acetyl CoA levels in IL12-stimulated $CD8^+$ T cells were, in part, due to the high expression of ACLY, which catalyzes the generation of acetyl CoA and oxaloacetate from citrate and CoA. Earlier studies have shown that *Acly* is a transcriptional target of *Srebp1* (51). We also observed an increased expression of *Srebp1* in IL12-stimulated $CD8^+$ T cells, corroborating high *Acly* expression in these cells. These data indicate that $CD8^+$ T cells activated in IL12 have an active malate–citrate shuttle that supports their intracellular acetyl CoA pool, similar to what was reported in cytokine-stimulated natural killer cells (52). Therefore, we envisaged that one of the critical roles of the malate–citrate cycle in IL12-stimulated $CD8^+$ T cells was to provide acetyl CoA for lipid synthesis. We based this on the observation that IL12-stimulated $CD8^+$ T cells displayed high neutral lipid content as compared with IL2-stimulated cells. Moreover, IL12-stimulated $CD8^+$ T cells also had elevated expression of genes, including *Fasn, Acaca, Scd1*, and *Scd2*, which encode *de novo* fatty acid synthesis enzymes. In addition, histone acetylation-mediated increased accessibility of genes could also account for increased expression of fatty acid synthesis genes in IL12-stimulated $CD8^+$ T cells. A recent study has shown that increased histone acetylation (H3K9Ac, H3K14Ac, and H3K56Ac) at the promoters of *Fasn* and *Acaca* leads to their increased transcription in HepG2 cells treated with acetate (53). However, further studies are needed to explore this possibility.

Most intriguingly, our RNA-seq analysis revealed that genes encoding fatty acid biosynthesis are primarily enriched in IL12-stimulated $CD8^+$ T cells when exposed to TCM, indicating their reliance on lipid metabolism to meet their bioenergetic demands in nutrient-restricted conditions. This is congruent with the observation that inhibition of lipolysis in IL12-stimulated $CD8^+$ T cells during exposure to TCM severely impinges on their viability. A similar phenomenon has also been reported in long-lasting memory and antitumor $CD8^+$ T cells, suggesting that lipolysis can be used as an alternative energy source for T cells in starved conditions (33, 34). We proposed that the increased lipolysis in IL12-stimulated $CD8^+$ T cells could be partly due to the lower expression of *Pprg*, which has been shown to negatively regulate the lipolysis (Supplementary Table S1; refs. 34, 54).

Finally, we found that the key metabolic features of IL12-stimulated $CD8^+$ T cells can be imprinted in $CD8^+$ T cells simply by augmenting their mitochondrial pyruvate oxidation by culturing the cells in high pyruvate–containing media without glucose. The reason for selecting such a condition was to ensure efficient fueling of mitochondrial TCA cycle with pyruvate so that concomitant an increase in acetyl CoA pool could be attained. Because different metabolic pathways with a discrete role in T-cell fate and function can be branched out from glycolysis, we thought of using glucose-free conditions to activate these cells. We argue that in addition to acetyl CoA–dependent acquisition of metabolic and functional fitness, glucose restriction could also aid in improving the overall antitumor potential of IL2 Py $CD8^+$ T cells, as reported in earlier studies (10). On the basis of our observation, we propose that strategies elevating intracellular acetyl CoA pool in $CD8^+$ T cells through boosted pyruvate oxidation in mitochondria would be an affordable approach for generating antitumor T cells for adoptive cell therapy.

Authors' Disclosures

A. Mukhopadhyay reports other support from Royalty outside the submitted work. No disclosures were reported by the other authors.

Authors' Contributions

S. Chowdhury: Conceptualization, data curation, formal analysis, investigation, writing–original draft. **A. Kar:** Data curation, formal analysis. **D. Bhowmik:** Formal analysis, methodology. **A. Gautam:** Software, formal analysis, methodology. **D. Basak:** Data curation, investigation. **I. Sarkar:** Data curation, methodology. **P. Ghosh:** Investigation, methodology. **D. Sarkar:** Data curation, methodology. **A. Deka:** Resources. **P. Chakraborty:** Resources. **A. Mukhopadhyay:** Resources. **S. Mehrotra:** Resources. **S. Basak:** Resources, writing–review and editing. **S. Paul:** Software, formal analysis, methodology, writing–review and editing. **S. Chatterjee:** Conceptualization, formal analysis, supervision, funding acquisition, writing–original draft, writing–review and editing.

Acknowledgments

The work was partially supported in part by DBT/Wellcome Trust India Alliance Intermediate Fellowship grant IA/I/19/1/504277 and SERB extramural fund CRG/2019/001334/BHS (to S. Chatterjee). S. Paul was supported by the Ramanujan Fellowship of Science and Engineering Research Board (SERB), Government of India. S. Chowdhury, A. Kar, D. Basak, and I. Sarkar are the recipients of the CSIR-Senior Research Fellowship. D. Bhowmik is the recipient of the ICMR-Senior Research Fellowship. NIH RO1 CA236379 and RO1 CA250458 supported S. Mehrotra.

The costs of publication of this article were defrayed in part by the payment of page charges. This article must therefore be hereby marked *advertisement* in accordance with 18 U.S.C. Section 1734 solely to indicate this fact.

Received November 25, 2021; revised April 20, 2022; accepted May 20, 2022; published first May 31, 2022.

References

1. Wei SC, Duffy CR, Allison JP. Fundamental mechanisms of immune checkpoint blockade therapy. Cancer Discov 2018;8:1069–86.
2. Morotti M, Albukhari A, Alsaadi A, Artibani M, Brenton JD, Curbishley SM, et al. Promises and challenges of adoptive T-cell therapies for solid tumours. Br J Cancer 2021;124:1759–76.
3. Sharma P, Allison JP. The future of immune checkpoint therapy. Science 2015;348:56–61.
4. Zarour HM. Reversing T-cell dysfunction and exhaustion in cancer. Clin Cancer Res 2016;22:1856–64.
5. DePeaux K, Delgoffe GM. Metabolic barriers to cancer immunotherapy. Nat Rev Immunol 2021;21:785–97.
6. Gajewski TF, Schreiber H, Fu YX. Innate and adaptive immune cells in the tumor microenvironment. Nat Immunol 2013;14:1014–22.
7. Buck MD, Sowell RT, Kaech SM, Pearce EL. Metabolic instruction of immunity. Cell 2017;169:570–86.
8. Chang CH, Curtis JD, Maggi LB Jr, Faubert B, Villarino AV, O'Sullivan D, et al. Posttranscriptional control of T-cell effector function by aerobic glycolysis. Cell 2013;153:1239–51.

9. Zhao E, Maj T, Kryczek I, Li W, Wu K, Zhao L, et al. Cancer mediates effector T-cell dysfunction by targeting microRNAs and EZH2 via glycolysis restriction. Nat Immunol 2016;17:95–103.
10. Klein Geltink RI, Edwards-Hicks J, Apostolova P, O'Sullivan D, Sanin DE, Patterson AE, et al. Metabolic conditioning of CD8(+) effector T cells for adoptive cell therapy. Nat Metab 2020;2:703–16.
11. Klein Geltink RI, O'Sullivan D, Corrado M, Bremser A, Buck MD, Buescher JM, et al. Mitochondrial priming by CD28. Cell 2017;171:385–97.
12. O'Sullivan D, Sanin DE, Pearce EJ, Pearce EL. Metabolic interventions in the immune response to cancer. Nat Rev Immunol 2019;19:324–35.
13. Colombo MP, Trinchieri G. Interleukin-12 in antitumor immunity and immunotherapy. Cytokine Growth Factor Rev 2002;13:155–68.
14. Leonard JP, Sherman ML, Fisher GL, Buchanan LJ, Larsen G, Atkins MB, et al. Effects of single-dose interleukin-12 exposure on interleukin-12–associated toxicity and interferon-gamma production. Blood 1997;90:2541–8.
15. Nguyen KG, Vrabel MR, Mantooth SM, Hopkins JJ, Wagner ES, Gabaldon TA, et al. Localized interleukin-12 for cancer immunotherapy. Front Immunol 2020;11:575597.
16. Garris CS, Arlauckas SP, Kohler RH, Trefny MP, Garren S, Piot C, et al. Successful anti–PD-1 cancer immunotherapy requires T-cell dendritic cell crosstalk involving the cytokines IFN-gamma and IL12. Immunity 2018;49:1148–61.
17. Chang S, Aune TM. Dynamic changes in histone-methylation "marks" across the locus encoding interferon-gamma during the differentiation of T helper type 2 cells. Nat Immunol 2007;8:723–31.
18. Smith CA, Want EJ, O'Maille G, Abagyan R, Siuzdak G. XCMS: processing mass spectrometry data for metabolite profiling using nonlinear peak alignment, matching, and identification. Anal Chem 2006;78:779–87.
19. Baumeister TUH, Ueberschaar N, Schmidt-Heck W, Mohr JF, Deicke M, Wichard T, et al. DeltaMS: a tool to track isotopologues in GC- and LC-MS data. Metabolomics 2018;14:41.
20. Wishart DS, Tzur D, Knox C, Eisner R, Guo AC, Young N, et al. HMDB: the human metabolome database. Nucleic Acids Res 2007;35:D521–6.
21. Dobin A, Davis CA, Schlesinger F, Drenkow J, Zaleski C, Jha S, et al. STAR: ultrafast universal RNA-seq aligner. Bioinformatics 2013;29:15–21.
22. Liao Y, Smyth GK, Shi W. The R package Rsubread is easier, faster, cheaper and better for alignment and quantification of RNA sequencing reads. Nucleic Acids Res 2019;47:e47.
23. Lawrence M, Huber W, Pages H, Aboyoun P, Carlson M, Gentleman R, et al. Software for computing and annotating genomic ranges. PLoS Comput Biol 2013;9:e1003118.
24. Love MI, Huber W, Anders S. Moderated estimation of fold change and dispersion for RNA-seq data with DESeq2. Genome Biol 2014;15:550.
25. McCarthy DJ, Chen Y, Smyth GK. Differential expression analysis of multifactor RNA-Seq experiments with respect to biological variation. Nucleic Acids Res 2012;40:4288–97.
26. Chatterjee S, Thyagarajan K, Kesarwani P, Song JH, Soloshchenko M, Fu J, et al. Reducing CD73 expression by IL1beta-programmed Th17 cells improves immunotherapeutic control of tumors. Cancer Res 2014;74:6048–59.
27. Pearce EL, Mullen AC, Martins GA, Krawczyk CM, Hutchins AS, Zediak VP, et al. Control of effector $CD8^+$ T-cell function by the transcription factor Eomesodermin. Science 2003;302:1041–3.
28. Muir A, Danai LV, Gui DY, Waingarten CY, Lewis CA, Vander Heiden MG. Environmental cystine drives glutamine anaplerosis and sensitizes cancer cells to glutaminase inhibition. Elife 2017;6:e27713.
29. Borges da Silva H, Beura LK, Wang H, Hanse EA, Gore R, Scott MC, et al. The purinergic receptor P2RX7 directs metabolic fitness of long-lived memory CD8(+) T cells. Nature 2018;559:264–8.
30. Cannarile MA, Lind NA, Rivera R, Sheridan AD, Camfield KA, Wu BB, et al. Transcriptional regulator Id2 mediates $CD8^+$ T-cell immunity. Nat Immunol 2006;7:1317–25.
31. Ding ZC, Shi H, Aboelella NS, Fesenkova K, Park EJ, Liu Z, et al. Persistent STAT5 activation reprograms the epigenetic landscape in CD4(+) T cells to drive polyfunctionality and antitumor immunity. Sci Immunol 2020;5:eaba5962.
32. Zheng WP, Zhao Q, Zhao X, Li B, Hubank M, Schatz DG, et al. Up-regulation of Hlx in immature Th cells induces IFN-gamma expression. J Immunol 2004;172:114–22.
33. O'Sullivan D, van der Windt GJW, Huang SC, Curtis JD, Chang CH, Buck MD, et al. Memory CD8(+) T cells use cell-intrinsic lipolysis to support the metabolic programming necessary for development. Immunity 2018;49:375–6.
34. Chakraborty P, Vaena SG, Thyagarajan K, Chatterjee S, Al-Khami A, Selvam SP, et al. Pro-survival lipid sphingosine-1-phosphate metabolically programs T cells to limit antitumor activity. Cell Rep 2019;28:1879–93.
35. Hutloff A, Dittrich AM, Beier KC, Eljaschewitsch B, Kraft R, Anagnostopoulos I, et al. ICOS is an inducible T-cell co-stimulator structurally and functionally related to CD28. Nature 1999;397:263–6.
36. Patterson SJ, Han JM, Garcia R, Assi K, Gao T, O'Neill A, et al. Cutting edge: PHLPP regulates the development, function, and molecular signaling pathways of regulatory T cells. J Immunol 2011;186:5533–7.
37. Chatterjee S, Daenthanasanmak A, Chakraborty P, Wyatt MW, Dhar P, Selvam SP, et al. CD38-NAD(+)axis regulates immunotherapeutic antitumor T-cell response. Cell Metab 2018;27:85–100.
38. Lu W, Zhang Y, McDonald DO, Jing H, Carroll B, Robertson N, et al. Dual proteolytic pathways govern glycolysis and immune competence. Cell 2014;159:1578–90.
39. Kiritsy MC, McCann K, Mott D, Holland SM, Behar SM, Sassetti CM, et al. Mitochondrial respiration contributes to the interferon gamma response in antigen-presenting cells. Elife 2021;10:e65109.
40. Bailis W, Shyer JA, Zhao J, Canaveras JCG, Al Khazal FJ, Qu R, et al. Distinct modes of mitochondrial metabolism uncouple T-cell differentiation and function. Nature 2019;571:403–7.
41. Riganti C, Gazzano E, Polimeni M, Aldieri E, Ghigo D. The pentose phosphate pathway: an antioxidant defense and a crossroad in tumor cell fate. Free Radic Biol Med 2012;53:421–36.
42. Watson JA, Fang M, Lowenstein JM. Tricarballylate and hydroxycitrate: substrate and inhibitor of ATP: citrate oxaloacetate lyase. Arch Biochem Biophys 1969;135:209–17.
43. Lu C, Thompson CB. Metabolic regulation of epigenetics. Cell Metab 2012;16:9–17.
44. Gubser PM, Bantug GR, Razik L, Fischer M, Dimeloe S, Hoenger G, et al. Rapid effector function of memory $CD8^+$ T cells requires an immediate-early glycolytic switch. Nat Immunol 2013;14:1064–72.
45. Peng M, Yin N, Chhangawala S, Xu K, Leslie CS, L MO. Aerobic glycolysis promotes T helper 1 cell differentiation through an epigenetic mechanism. Science 2016;354:481–4.
46. Fann M, Godlove JM, Catalfamo M, Wood WH III, Chrest FJ, Chun N, et al. Histone acetylation is associated with differential gene expression in the rapid and robust memory CD8(+) T-cell response. Blood 2006;108:3363–70.
47. Zaidi N, Swinnen JV, Smans K. ATP-citrate lyase: a key player in cancer metabolism. Cancer Res 2012;72:3709–14.
48. Chang CH, Qiu J, O'Sullivan D, Buck MD, Noguchi T, Curtis JD, et al. Metabolic competition in the tumor microenvironment is a driver of cancer progression. Cell 2015;162:1229–41.
49. Wang T, Liu G, Wang R. The intercellular metabolic interplay between tumor and immune cells. Front Immunol 2014;5:358.
50. Ylikoski E, Lund R, Kylaniemi M, Filen S, Kilpelainen M, Savolainen J, et al. IL12 upregulates T-bet independently of IFN-gamma in human $CD4^+$ T cells. Eur J Immunol 2005;35:3297–306.
51. Sato R, Okamoto A, Inoue J, Miyamoto W, Sakai Y, Emoto N, et al. Transcriptional regulation of the ATP citrate-lyase gene by sterol regulatory element-binding proteins. J Biol Chem 2000;275:12497–502.
52. Assmann N, O'Brien KL, Donnelly RP, Dyck L, Zaiatz-Bittencourt V, Loftus RM, et al. Srebp-controlled glucose metabolism is essential for NK cell functional responses. Nat Immunol 2017;18:1197–206.
53. Gao X, Lin SH, Ren F, Li JT, Chen JJ, Yao CB, et al. Acetate functions as an epigenetic metabolite to promote lipid synthesis under hypoxia. Nat Commun 2016;7:11960.
54. Picard F, Kurtev M, Chung N, Topark-Ngarm A, Senawong T, Machado De Oliveira R, et al. Sirt1 promotes fat mobilization in white adipocytes by repressing PPAR-gamma. Nature 2004;429:771–6.